

Ferroelectric nematicogens containing a methylthio group.

STEPANAFAS, G., CRUICKSHANK, E., BROWN, S., MAJEWSKA, M.M., POCHIECHA, D., GORECKA, E., STOREY, J.M.D. and IMRIE, C.T.

2024

Supplementary materials are appended after the main text of this document.



Cite this: *Mater. Adv.*, 2024,
5, 525

Ferroelectric nematogens containing a methylthio group†

Gytis Stepanafas,^{ib a} Ewan Cruickshank,^{ib ‡*a} Stevie Brown,^{ib a}
Magdalena M. Majewska,^{ib b} Damian Pociecha,^{ib b} Ewa Gorecka,^{ib b}
John M.D. Storey^{ib a} and Corrie T. Imrie^{ib a}

The synthesis and characterisation of eight nematogens containing a terminal methylthio group is reported. The compounds are based on RM734 and differ in the number and position of fluorine substituents, and in the position of the lateral methoxy substituent. Seven of these compounds exhibit a monotropic ferroelectric nematic phase, N_F , including examples of N_F -isotropic phase transitions. Two of the compounds show the anti-ferroelectric N_X phase. Their transitional behaviour is discussed in terms of molecular shape and changes in electronic properties. Their phase behaviour is similar to that of the corresponding compounds containing a terminal methoxy group, but the methoxy terminated materials consistently show the higher transition temperatures. This is accounted for by the larger reduction in molecular shape anisotropy associated with the methylthio group, and the associated change in the electronic properties. The N_X phase seen for the methylthio substituted compounds are thought to reflect the suppression of the N_F phase by the methylthio group rather than any specific stabilising effect. Specific interactions between methylthio groups thought to stabilise nematic behaviour do not appear to stabilise the N_F phase.

Received 21st July 2023,
Accepted 14th October 2023

DOI: 10.1039/d3ma00446e

rsc.li/materials-advances

Introduction

The ferroelectric nematic phase, N_F , was experimentally discovered in 2017,^{1–3} and is now the hottest topic in liquid crystal research. In the conventional nematic phase, N , the rod-like molecules are more or less aligned along a common direction, the director, whereas their centres of mass are distributed randomly. The director is described by a unit vector, \mathbf{n} , which possesses inversion symmetry such that $\mathbf{n} = -\mathbf{n}$, and the phase is apolar, Fig. 1. In the N_F phase, the director no longer possesses inversion symmetry *i.e.* $\mathbf{n} \neq -\mathbf{n}$, and the phase is polar, Fig. 1.⁴ This phase has generated very significant excitement not only given the fundamental importance of a fluid ferroelectric phase, but also because it has huge application potential in a range of electrooptic technologies. A small number of materials exhibit a further liquid crystal phase referred to as the N_X or SmZ_A phase.^{2,5–8} The N_X phase is thought to consist of regions of polar nematic phase arranged in a regular antiferroelectric structure.^{5,7,9}

To date there have been around 150 molecules reported to show the N_F phase and bar a handful of exemptions such as polymers,^{10,11} these materials may be described as conventional low molar mass mesogens.^{3,6,8,12–25} The empirical structure–property relationships describing the links between the formation of the N_F phase and molecular structure have yet to be established let alone understood. The archetypal ferroelectric nematic compounds RM734³ and DIO² have large longitudinal dipole moments and possess lateral bulk in the form of either a methoxy group or fluorine substituents. It has been

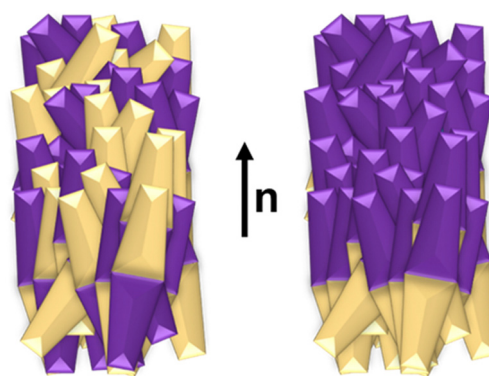


Fig. 1 Schematic representations of the conventional nematic, N , phase (left) and ferroelectric nematic, N_F , phase (right).

^a Department of Chemistry, University of Aberdeen, Old Aberdeen, AB24 3UE, UK.
E-mail: ewan.cruickshank2@abdn.ac.uk

^b Faculty of Chemistry, University of Warsaw, ul. Zwirki i Wigury 101, 02-089,
Warsaw, Poland

† Electronic supplementary information (ESI) available. See DOI: <https://doi.org/10.1039/d3ma00446e>

‡ Present Address: School of Pharmacy and Life Sciences, Robert Gordon University, Aberdeen, AB10 7GJ, U.K.



suggested that these structural factors are prerequisites for the observation of the N_F phase. Indeed, this view is supported by computer simulations of tapered Gay–Berne particles possessing longitudinal dipole moments that revealed N_F behaviour.²⁶ Exceptions have been reported to these generalisations (see, for example, ref. 18,24,27), and in order to design new ferroelectric nematogens having tailored properties in a rational manner we must first explore and understand the relationships between structure and properties for the N_F phase.

Sulfur has been used extensively in the design of liquid crystals including, for example, in terminal alkylthio chains,^{28–34} alkylthio spacers,^{35–40} thiophene moieties,^{41–44} thiocyanate terminal groups,^{45,46} and thioester linking groups.^{47,48} One driving force for this research is the enhanced values of optical birefringence exhibited by compounds that contain sulfur.^{45,49–52} Highly birefringent nematogens have considerable application potential not only in liquid crystal display technologies, but also have an important role to play in emerging technologies such as liquid crystal lenses^{53,54} and as holographic materials.⁵⁵ Surprisingly, sulfur has very largely been overlooked in the design of ferroelectric nematogens, and to address this surprising omission, here we report the synthesis and characterisation of eight new compounds, **S1–8**, designed to exhibit the N_F phase and that contain a methylthio substituent, Table 1. These are based on the archetypal ferroelectric nematogen RM734.³ The properties of these compounds are compared with those of the corresponding materials in which the methylthio group has been replaced by a methoxy unit, **O1–8**, Table 1. We note that **O1** is RM734. Critically, this is the first time that specifically the effect of replacing the terminal methoxy group with a terminal methylthio group on the formation of the N_F phase has been studied, while also sequentially changing the degree of fluorination incorporated into the molecular backbone.

Experimental

Synthesis

The synthetic route used to prepare **S1–8** is shown in Scheme 1 and for **O5** and **O6** in Scheme 2. A detailed description of the preparation of these compounds, including the structural characterisation data for all intermediates and final products, is provided in the Supplementary Information.

Optical studies

Phase characterisation was performed by polarised light microscopy, using an Olympus BH2 polarising light microscope equipped with a Linkam TMS 92 hot stage. Slides treated for planar alignment were purchased from INSTEC or AWAT with a thickness between 2.9–3.5 μm or 1.8 μm , respectively and both sets of cells were ITO conducting.

Differential scanning calorimetry

The phase behaviour of the materials was studied by differential scanning calorimetry performed using a Mettler Toledo DSC1 or DSC3 differential scanning calorimeter equipped with TSO 801RO sample robots and calibrated using indium and

zinc standards. Heating and cooling rates were 10 K min^{-1} , with a 3 min isotherm between either heating or cooling, and all samples were measured under a nitrogen atmosphere. Transition temperatures and associated enthalpy changes were extracted from the heating traces unless otherwise noted. For each sample, two aliquots were measured, and the data listed are the average of the two sets of data.

Molecular modelling

The geometric parameters of the reported compounds were obtained using quantum mechanical DFT calculations with Gaussian09 software.⁵⁶ Optimisation of the methylthio-containing structures (**S1–8**) was carried out at the B3LYP/6-311G(d,p) level of theory. Comparison of the results of optimisation of the corresponding ether-linked (**O1–8**) materials at the B3LYP/6-311G(d,p) and the 6-31G(d) levels showed no discernible difference in the geometries found, and so their optimisation was carried out at the B3LYP/6-31G(d) level. Visualisations of the electronic surfaces were generated from the optimised geometries using the GaussView 5 software, and visualisations of the space-filling models were produced post-optimisation using the QuteMol package.⁵⁷

Birefringence measurements

Birefringence was measured with a setup based on a photoelastic modulator (PEM-90, Hinds) working at a modulation frequency $f = 50$ kHz; as a light source, a halogen lamp (Hamamatsu LC8) was used equipped with narrow bandpass filters (633 nm and 690 nm). The signal from a photodiode (FLC Electronics PIN-20) was deconvoluted with a lock-in amplifier (EG&G 7265) into $1f$ and $2f$ components to yield a retardation induced by the sample. Knowing the sample thickness, the retardation was recalculated into optical birefringence. Samples were prepared in 4.9-micron-thick cells with planar anchoring. The alignment quality was checked prior to measurement by inspection under the polarised light optical microscope.

Spontaneous electric polarization measurements

Values of the spontaneous electric polarization were obtained from the current peaks recorded during P_s switching upon applying a triangular-wave voltage at a frequency of 2 Hz. The 9.7 μm -thick cells with ITO electrodes and no polymer aligning layers were used and the switching current was determined by recording the voltage drop at the resistivity of 50 $\text{k}\Omega$ in serial connection with the sample. The current peak was integrated over time to calculate the surface electric charge and evaluate the polarization value.

Dielectric spectroscopy

The complex dielectric permittivity, ϵ^* , was studied using a Solatron 1260 impedance analyser. Measurements were conducted in the 1 Hz–1 MHz frequency (f) range, with the probe voltage of 20 mV, and it was checked by optical observations that such a voltage is below the Fredericks transition threshold. The material was placed in 9.7 μm -thick glass cells with ITO electrodes and no polymer aligning layers. Lack of a surfactant



Table 1 Molecular structures of the *S_n* and *O_n* compounds

Name	Structure	Name	Structure
S1		O1	
S2		O2	
S3		O3	
S4		O4	
S5		O5	
S6		O6	
S7		O7	
S8		O8	

layer resulted in the random configuration of the director in the LC phases; microscopic observations of optical textures suggested a dominant planar orientation without preferable direction of the long molecular axis. The relaxation frequency, f_r , and dielectric strength of the mode, $\Delta\epsilon$, were evaluated by fitting the complex dielectric permittivity to the Cole–Cole formula:

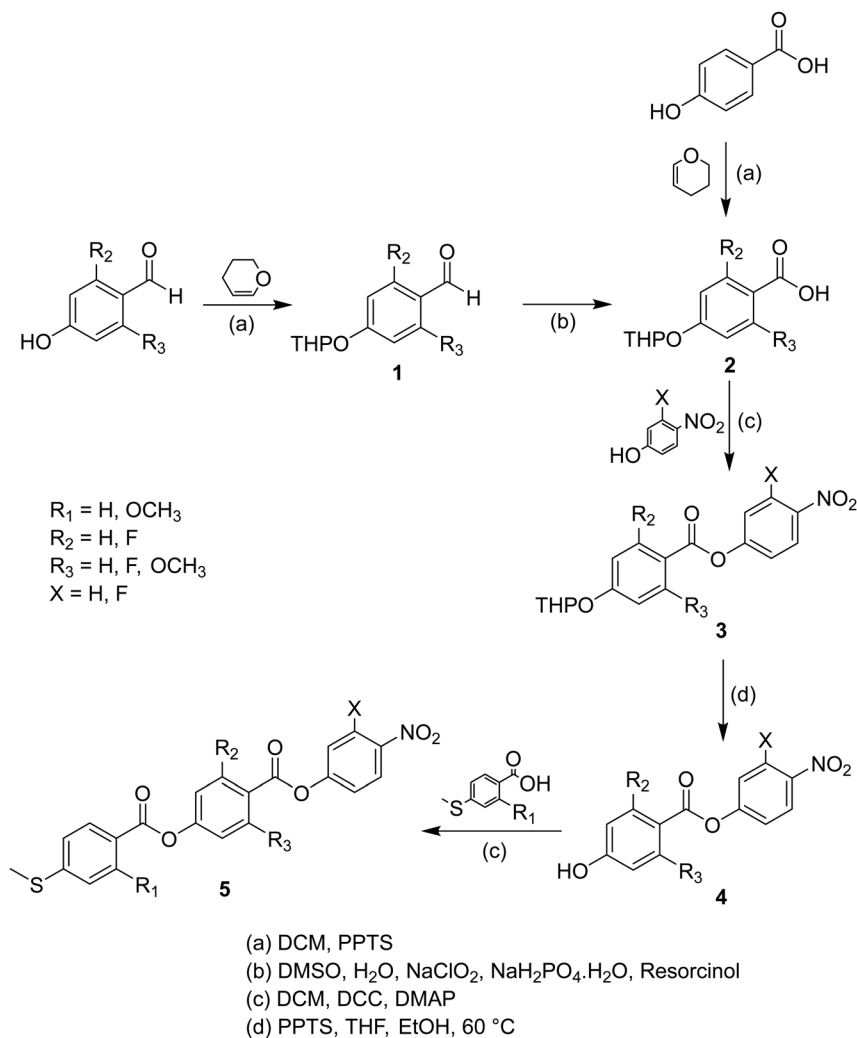
$$\epsilon - \epsilon_\infty = \sum \frac{\Delta\epsilon}{\left(1 + \frac{if}{f_r}\right)^{1-\alpha}} + i\left(\frac{\delta}{2\pi\epsilon_0 f}\right),$$

where ϵ_∞ is the high frequency dielectric constant, α is the distribution parameter of the mode and δ is the low frequency conductivity, respectively.

X-ray diffraction

The X-ray diffraction (XRD) measurements were performed with a Bruker D8 GADDS system (CuK α line, Goebel mirror, point beam collimator, Vantec2000 area detector). The temperature of the sample was controlled with precision of ± 0.1 K. Samples were prepared as droplets on a heated surface.





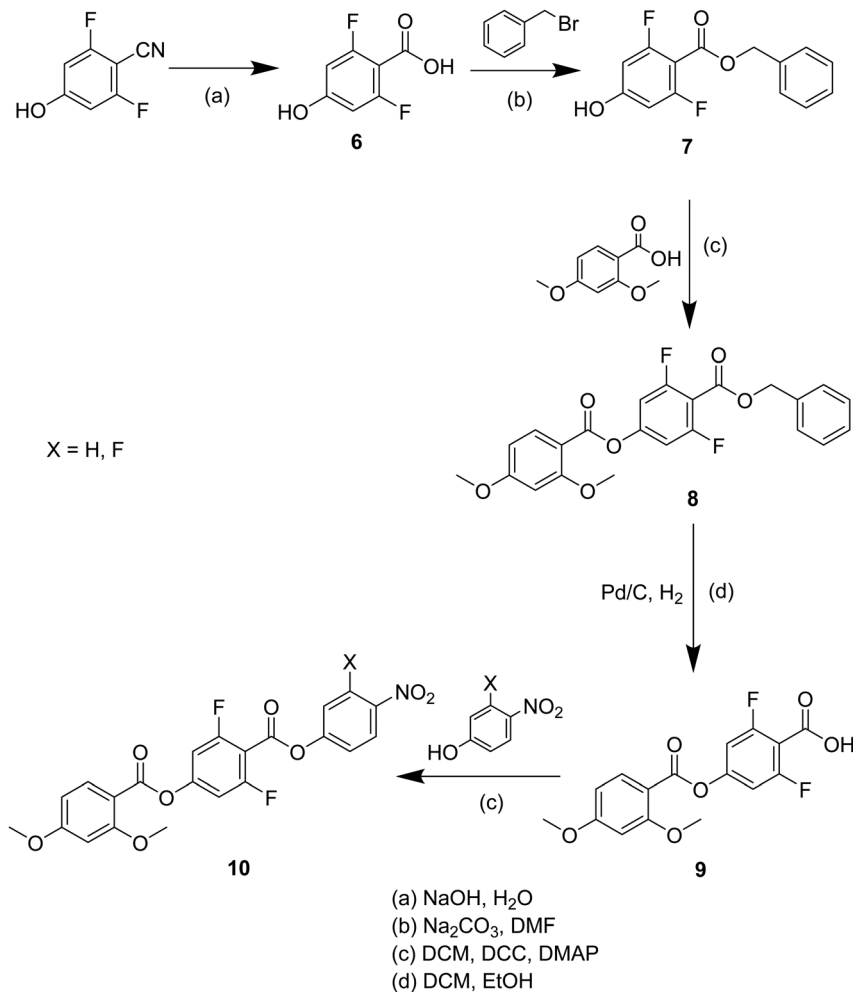
Scheme 1 Synthetic route used to obtain the *S_n* compounds.

Results and discussion

The transitional properties of the methylthio-containing *S_n* materials are listed in Table 2. The conventional nematic phase, N, was assigned based on the observation of a characteristic uniform texture in a cell treated for planar alignment, Fig. 2(a), or on the observation of a characteristic schlieren texture containing two- and four-brush point defects when the sample was sandwiched between two untreated glass slides, Fig. 3(a). These textures flashed when subjected to mechanical stress. For **S1** and **S7** on cooling the uniform texture of the nematic phase, a chevron pattern was observed at the transition to the *N_x* phase, Fig. 2(b). In XRD studies (these will be discussed in more detail later) the *N_x* phase shows only short-range correlations of the molecular positions which are characteristic for nematic phases and hence why the phase is named as such. However, in previous diffraction experiments performed at synchrotron facilities very weak Bragg-type diffraction signals were detected in the *N_x* phase,⁹ revealing a kind of long-range periodicity. This periodicity was attributed to

existence of regular domains with antiparallel orientation of the polarization, and so this phase is referred to by other groups as the antiferroelectric *SmZ_A* phase.^{5–7} Cooling **S1** from the *N_x* phase saw a series of twisted states emerge a few degrees below the transition to the *N_F* phase, Fig. 2(c)–(e), and we have previously reported observing these textures for the *N_F* phase.⁸ There was also a clear change in birefringence which is also considered characteristic of the *N_F* phase. In **S4** and **S6**, the *N_F* phase formed directly from the isotropic phase. In thicker cells treated for planar alignment, spherical droplets developed at the *N_F*-I transition and coalesced to form banded textures which are also characteristic of the *N_F* phase, Fig. 3(b) and (c).^{10,13,18,20,25} This banded texture is observed due to the domains which form within the cell separated by distinct domain boundaries. These domains show regions in which the director has different orientations and so the polarisation direction is similarly changed. The banding within the domains is due to areas of lower and higher birefringence, with the domains themselves thought to form due to director splay deformations which are necessary to connect opposite polarisation vectors on the lower and upper



Scheme 2 Synthetic route used to obtain compounds **O5** and **O6**.Table 2 Transition temperatures for the *S_n* and *O_n* series (in °C) with their associated enthalpy changes (in parentheses, kJ mol⁻¹)

Compound	M.P.	Phase sequence
S1	147 (38.6)	I-169 (0.54)-N ^a -111 (^c 0.43)-N _X ^a -106 (^c 0.43)-N _F
S2	147 (43.9)	I ^a -135 (0.54)-N ^a -122 (1.29)-N _F
S3	162 (40.3)	I ^a -152 (0.41)-N ^a -126 (0.57)-N _F
S4	150 (36.0)	I ^a -129 (3.09)-N _F
S5	174 (47.8)	I ^a -127 (0.40)-N ^a -121 (0.80)-N _F
S6	171 (52.9)	I ^a -122 (3.56)-N _F
S7	164 (47.9)	I-172 (1.22)-N ^b -97-N _X
S8	164 (40.3)	I ^a -143 (0.74)-N ^a -124 (0.28)-N _F
^d O1	139 (34.3)	I-188 (0.61)-N-131 (0.60)-N _F
^e O2	166 (50.4)	I-155 (0.50)-N-140 (1.61)-N _F
^f O3	161 (54.1)	I-165 (0.69)-N-143 (1.38)-N _F
^f O4	151 (53.2)	I-139 (4.38)-N _F
O5	192 (50.6)	I ^a -139 (0.34)-N ^a -132 (1.62)-N _F
O6	160 (45.4)	I ^a -131 (4.33)-N _F
^g O7	192 (48.3)	I-189 (0.81)-N-126 (0.11)-N _F
^g O8	180 (51.6)	I-157 (10.4)-N-142 (1.17)-N _F

^a Values extracted from DSC cooling traces. ^b Measured using the polarised light microscope. ^c Combined ΔH value associated with both phase transitions due to peak overlap in the DSC trace. ^d Data extracted from Cruickshank *et al.*²⁰ ^e Data extracted from Mandle *et al.*³ ^f Data extracted from Brown *et al.*⁸ ^g Data extracted from Tufaha *et al.*¹⁸

cell surfaces.⁸ The scaled entropy changes, calculated using the enthalpy changes listed in Table 2, associated with the N_F-I transitions of **S4** and **S6** are several times larger than those associated with the N-I transitions, Table 2. This presumably reflects the additional entropic contribution associated with the ordering of the dipoles in the N_F phase compared to the conventional N phase. The values of the enthalpy changes listed in Table 2 are similar to those reported for other ferroelectric nematogens.^{8,12,18,20}

In order to confirm the phase assignments, dielectric measurements were undertaken using **S1**. In the N phase, a clear dielectric mode was found for which the relaxation frequency decreased and the strength increased on cooling, as the correlation length of polar order also increased. There was a clear increase in the value of ϵ upon entry to the N_F phase, Fig. 4. The low frequency dielectric strength was over 10 000 and this is in agreement with values reported for other ferroelectric nematogens.^{2,8,10,12,14-16,18,58-60} However, it has been recently reported that there may be a relationship between these values and the cell thickness.⁶¹ The polar character of the N_F phase was further confirmed by the polarisation switching behaviour. When an AC voltage was applied a



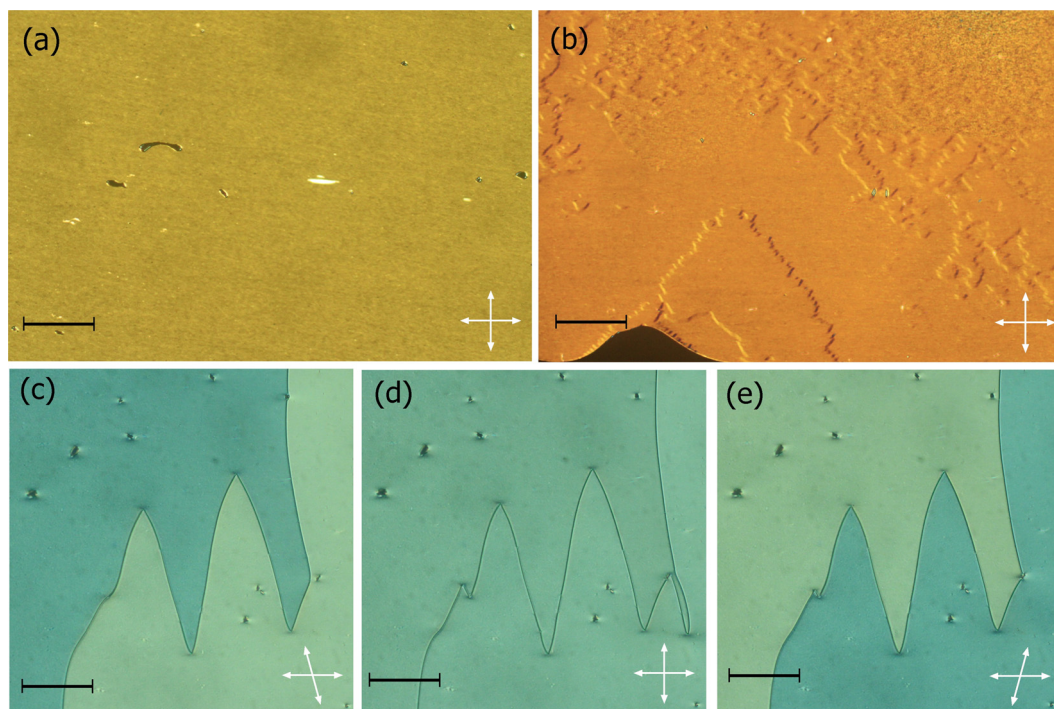


Fig. 2 Polarised optical microscope textures observed for the compound, **S1**: (a) uniform texture of the N phase at 130 °C; (b) chevron texture of the N_x phase at 110 °C; (c)–(e) twisted states of the N_F phase at 100 °C, with (d) showing the texture when the polarisers are fully crossed. All textures were obtained in cells treated for planar alignment with the scale bars each representing 200 μm .

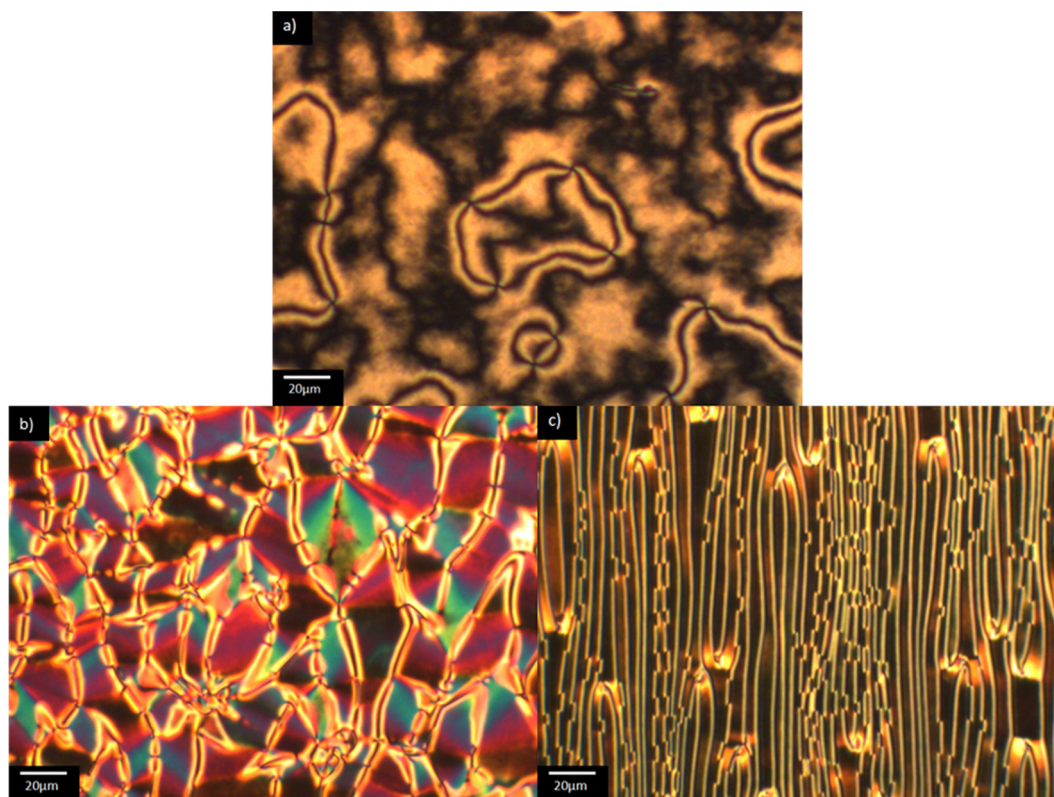


Fig. 3 Polarised optical microscope textures observed for the S_n series: (a) schlieren texture of the N phase viewed between untreated glass slides for **S2** at 130 °C; (b) banded texture of the N_F phase viewed in a cell treated for planar alignment for **S2** at 122 °C; and (c) banded texture of the N_F phase viewed in a cell treated for planar alignment for **S6** at 110 °C.



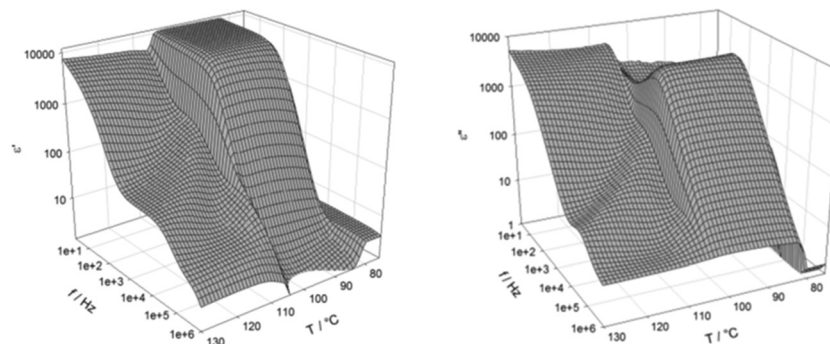


Fig. 4 Real (left) and imaginary (right) parts of the complex dielectric permittivity measured as a function of temperature and frequency for **S1**, in a 9.7 μm -thick cell with ITO electrodes and no alignment layer.

single current peak per half cycle was registered and this corresponded to a large spontaneous polarisation of $3.1 \mu\text{C cm}^{-2}$, Fig. 5, but only around half the value reported for RM734.⁴ Although these measurements gave a clear indication of **S1** exhibiting the ferroelectric nematic phase, they do not clearly reveal the N_x phase between the N and N_F phases that was seen using polarised light optical microscopy. The temperature dependence of the optical birefringence for **S1** is shown in Fig. 6. The optical studies showed that when the sample is cooled from the isotropic to the nematic phase, there is a sharp increase in the birefringence at the transition that then follows a critical power-law dependence. At the transition to the N_x phase there is a small change in the temperature dependence of birefringence showing that the phase is orientationally similar to the conventional nematic phase. This is followed by a small step-like increase at the transition to the N_F phase, indicative of an increase of the order parameter, S . This observation is in agreement with the birefringence measurements that we have reported previously for the N_x phase,^{8,9} also referred to as the smectic Z_A phase.^{5,62} Based on both the textural observations and this change in birefringence, the N_x phase in **S1** may be assigned as being the same phase shown by DIO and some related

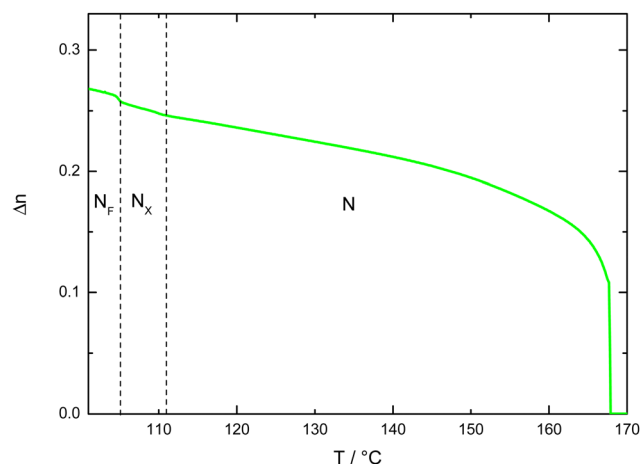


Fig. 6 Optical birefringence of **S1** measured with green light ($\lambda = 532 \text{ nm}$) across the phase transitions with the light green line showing the birefringence measured on cooling.

compounds.^{2,6,21} X-ray diffraction was also used to confirm the assignment of the phases in compound **S1** as nematics, Fig. 7. The X-ray diffraction patterns obtained for both the N and N_x phases are essentially identical consisting of broad signals indicative of there being only short-range correlations of the molecular positions. Prior to the observation of the N_F phase, however, the sample crystallised as shown by the observed diffraction pattern, Fig. 7 (c). The pattern seen for the N_x phase, although not showing the long-range periodicity we have reported previously,⁹ does support its assignment as a nematic phase.

We now turn our attention to the dependence of the transition temperatures on molecular structure for the methylthio-substituted compounds listed in Table 2. **S1**, the methylthio-substituted analogue of the extensively studied RM734, shows the phase sequence N_F - N_x -N-I, and forms the basis of comparison for compounds **S2–6** in which one, two or three fluorine substituents are added to the structure. In **S2** a fluorine substituent has been added *ortho* to the nitro group and this has reduced the nematic-isotropic transition temperature, T_{NI} , by 34 K. This decrease is presumably associated with the reduction in shape anisotropy. Conversely, the ferroelectric nematic-nematic transition temperature, T_{NFN} , of **S2** is 16 K higher than that of the N_F - N_x

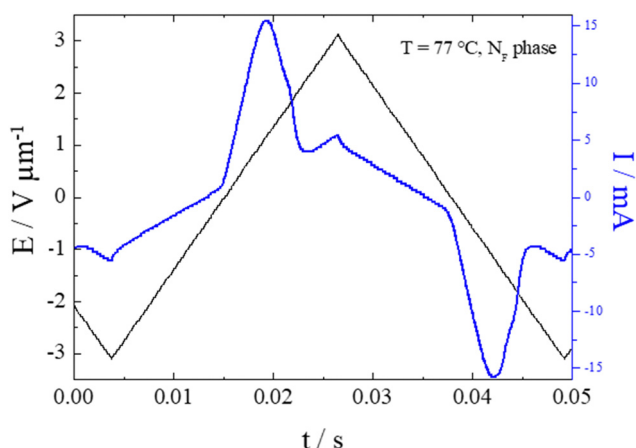


Fig. 5 The switching current (blue line) associated with polarization reversal under applied triangular wave voltage (black line) for **S1** at 77 °C. Measurements were performed in a 9.7 μm -thick cell with ITO electrodes and no alignment layer.



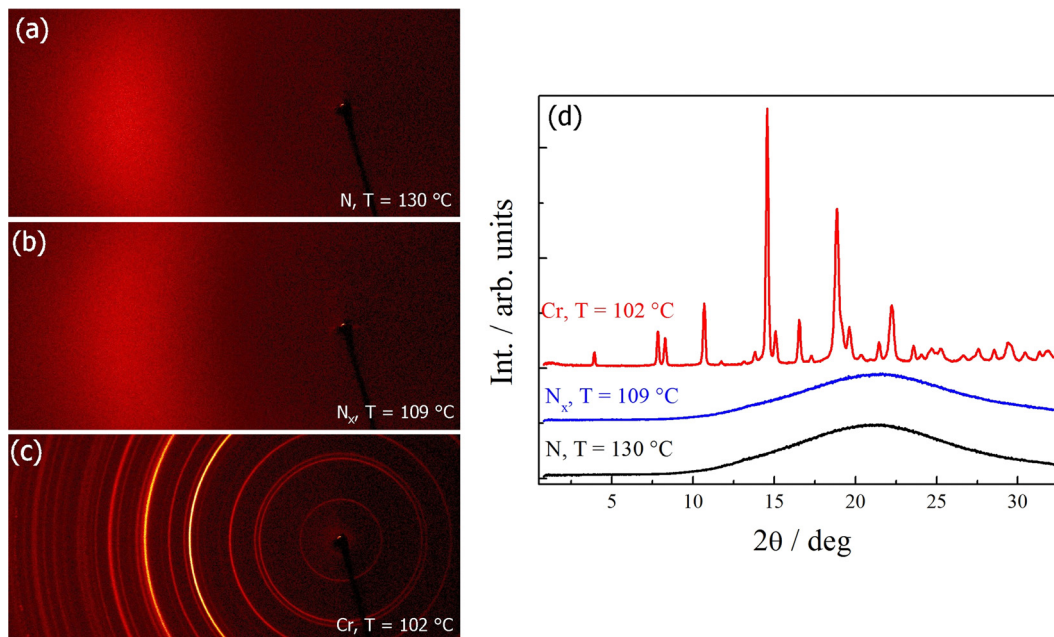


Fig. 7 X-ray diffraction patterns of compound **S1** in the (a) N phase; (b) N_x phase and (c) crystalline solid phase. (d) Intensity profiles of the X-ray patterns of the N phase (black line), N_x phase (blue line) and crystalline solid phase (red line).

transition temperature, T_{NFNX} observed for **S1**. This increase in the stability of the N_F phase may be attributed, in part, to an increase in the molecular dipole moment from 10.5 D for **S1** to 11.6 D for **S2**. It has also been suggested,¹⁸ however, that this observation is consistent with the predictions of a molecular model developed by Madhusudana to describe the N_F phase in which the molecules are described by a longitudinal surface charge density wave.⁶³ Specifically, the model suggests that the parallel alignment of the molecules is enhanced by minimising the amplitude of the charge density wave at either end of the molecule. The addition of the fluorine atom *ortho* to the nitro group spreads the electron charge distribution reducing the amplitude of the charge density wave, and so predicted to increase the stability of the N_F phase as observed.

In **S3** a fluorine atom has been added to the central phenyl ring in **S1** and this reduces T_{NI} by 17 K. This is a much smaller reduction in T_{NI} than seen between **S1** and **S2** of 34 K and reflects the different contributions to the molecular shape arising from substitutions in differing positions, Fig. 8. Again, the addition of a fluorine atom sees an increase in the stability of the N_F phase and T_{NFN} for **S3** is some 20 K higher than T_{NFNX} observed for **S1**. This is a larger difference than seen between the corresponding values of **S2** and **S1** although the dipole moment of **S3** is 11.2 D and lies between those of **S1** and **S2**. Indeed, T_{NFN} for **S3** is higher than that of **S2** although we note that this is a small difference, just 4 K. This supports the view that the stability of the N_F phase cannot be simply associated with the magnitude of the molecular dipole moment. Within Madhusudana's model, the addition of the fluorine atom increases the amplitude of the charge density on the central ring and in relative terms decreases that associated with the terminal rings. Such a change is predicted to increase the stability of the N_F phase.

S4 contains two fluorine substituents in the same positions as the individual fluorine atoms in **S2** and **S3**. This change has extinguished the nematic phase and a direct N_F -I transition is observed, corresponding to a reduction in T_{NI} of at least 40 K compared to **S1**. In contrast, the stability of the N_F has increased again and T_{NFI} for **S4** is 23 K higher than T_{NFNX} observed for **S1**. It is also noteworthy that T_{NFI} for **S4** is higher than T_{NFN} of **S2** by 7 K and of **S3** by 3 K. The dipole moment of **S4** is 12.4 D and higher than that of either **S2** or **S3**. It is clear that the effects of the two fluorine atoms on the stability of the N_F phase are not simply additive and such a relationship would predict a T_{NFI} for **S4** of around 142 °C. The rather modest increases in the stability of the N_F phase between **S4**, and **S2** and **S3** is not immediately apparent from Madhusudana's model. If the F-substituent in **S2** acts to reduce the amplitude of the charge density on the terminal ring, and that in **S3** increases the amplitude of the charge density on the middle ring, then the combined effect in **S4** should be to increase the difference between these two amplitudes, further increasing the stability of the N_F phase. Presumably the change in molecular shape must also be considered and this will not be simply additive, nor is it straightforward to assess.

S5 also contains two fluorine substituents but both are attached to the middle aromatic ring, and these have reduced T_{NI} by 42 K compared to **S1**. The single fluorine substituent on the middle ring in **S3** reduced T_{NI} by 17 K compared to **S1**, and so the second fluorine substituent has had a more pronounced effect on T_{NI} than the first, reducing T_{NI} by 25 K. The stability of the N_F phase shown by **S5** is higher than that of **S1**, but T_{NFN} is lower than that of **S3** by 5 K even though its dipole moment of 11.8 D is higher than that of **S3** of 11.2 D. These effects may be attributed to the change in molecular shape on the addition of



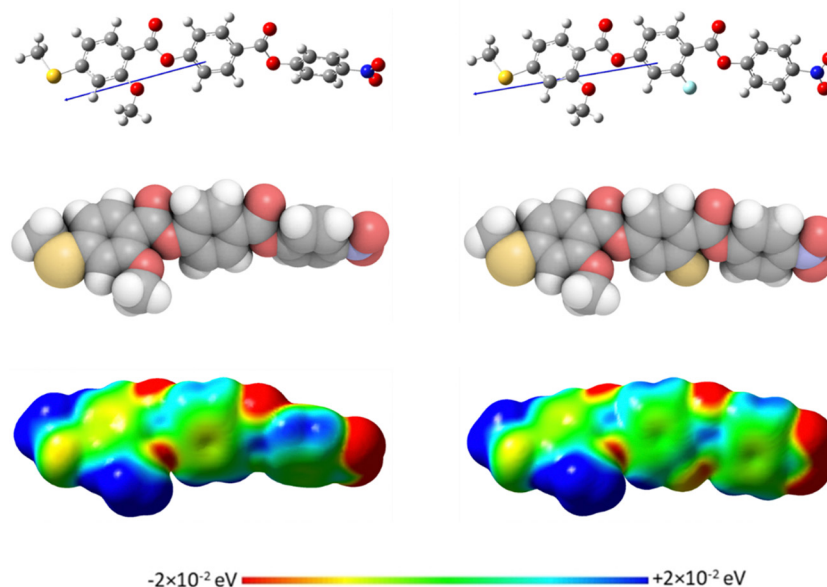


Fig. 8 Molecular modelling of: **S1** (left) and **S3** (right) calculated at the B3LYP/6-31(d) level of theory. The molecules are visualized using: (top) ball and stick models, (middle) space-filling models and (bottom) electrostatic potential surfaces. The arrow indicates the direction of the calculated dipole moment, with the head representing positive charge moving to the base which is negative.

the second fluorine substituent, and presumably this also spreads the electron distribution on the middle phenyl ring reducing the amplitude of the charge density wave relative to that of the terminal ring.

All three fluorine substituents are included in **S6**, and this has extinguished nematic behaviour in comparison to **S1** indicating a reduction in T_{NI} of at least 47 K. The value of T_{NFI} for **S6** is essentially the same as T_{NFI} shown by **S2** and **S5** although its dipole moment of 13.0 D is the highest in this collection of molecules. It is becoming increasingly apparent that the magnitude of the dipole moment alone is not a good indicator of the stability of the N_F phase. **S6** shows the largest reduction in T_{NI} compared to **S1** suggesting that the three fluorine substituents have a significant effect on molecular shape, and this presumably offsets a larger increase in the stability of the N_F phase based on the predicted increment in

stability associated with the addition of the fluorine substituent on the terminal phenyl ring.

For comparative purposes, the transitional properties of the corresponding methoxy-substituted materials to **S1–6**, the **O1–6** compounds are listed in Table 2 and their structures shown in Fig. 1. **O5** and **O6** were prepared as part of this study and their phase assignments based on the observation of a characteristic schlieren texture for the nematic phase, Fig. 9(a) and a banded texture for the N_F phase similar to that which we have reported previously, Fig. 9(b).^{18,20,25} For **O5** our studies have revealed a previously overlooked N phase and the characterisation data for this are provided in the ESI.† The remaining data have been extracted from the literature.^{3,8,18,20} The trends in phase behaviour within these two sets of compounds, **S1–6** and **O1–6**, are similar and tend to only differ in the magnitude of the temperature differences between compounds, Fig. 10. These

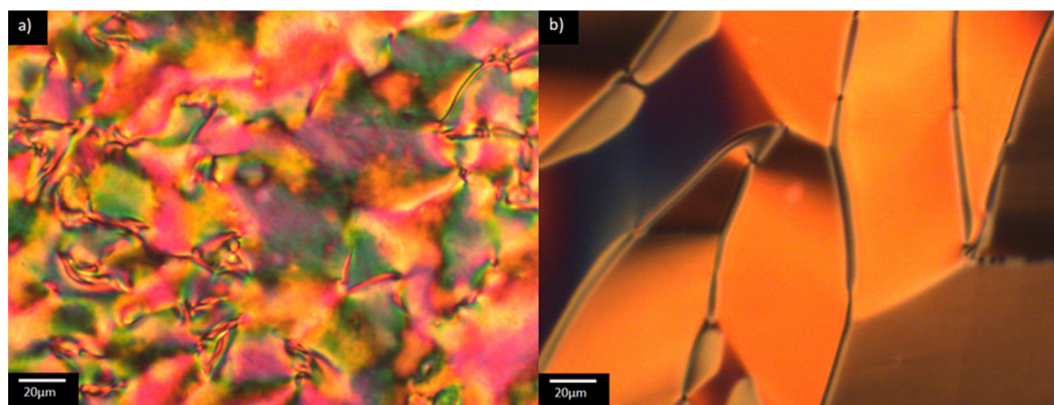


Fig. 9 Polarised optical microscope textures observed for **O6**: (a) highly birefringent texture of the N_F phase viewed between untreated glass slides at 125 °C; (b) banded texture of the N_F phase in a cell treated for planar alignment at 125 °C.



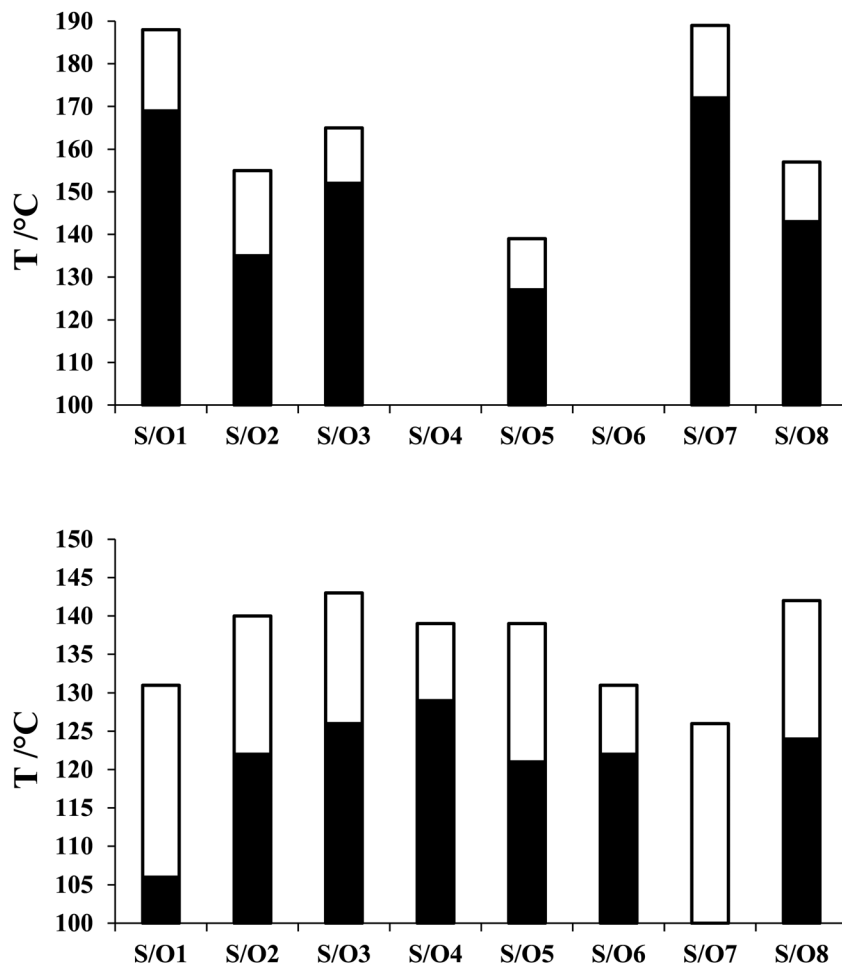


Fig. 10 Comparison of the N-I (top) and N_F-N/N_X/I (bottom) transition temperatures of the Sn series (filled bar) and On series (open bar).

temperature differences are most striking in the compounds containing more than one fluorine substituent for which the increase in the stability of the N_F phase is significantly larger in the Sn compounds. For example, the stability of the N_F phase shown by S6 is 16 K higher than that of S1, whereas the value of T_{NFI} shown by O6 is the same as that of T_{NFN} is for O1. This may reflect the weaker relative effect multiple fluorine substituents have on the shape of the Sn compounds given the larger methylthio group and we return to this issue later.

In S7 the methoxy substituent on the terminal ring has been moved to the middle ring and this increases T_{NI} by just 3 K compared to S1. This small change reflects the small change in the shape anisotropy of the molecule. By contrast, T_{NXN} has fallen by 14 K and the N_F phase is no longer observed for S7. This suggests that the addition of the methoxy unit to the middle ring has reduced the amplitude of the charge density wave given its electron donating character. As would be expected the addition of a fluorine substituent *ortho* to the nitro group giving S8 promotes N_F behaviour and reduces T_{NI} compared to S7, Fig. 10. Again, similar trends in behaviour are observed for the corresponding methoxy substituted materials O7 and O8, see Table 2. The N_X phase is again not observed in the On compounds.

The transitional behaviour of the corresponding Sn and On materials, Table 2, is identical except for the pairs S1 and O1 (RM734), and S7 and O7. In both S1 and S7 the N_X phase is observed but not seen in the corresponding O compounds. In addition, the N_F phase is not observed for S7 but is for O7. Indeed, isolated droplets of S7 can be cooled to 60 °C with no sign of a phase change within the N_X phase, implying a reduction in T_{NFN} of at least 66 K compared to O7. Comparing the transition temperatures of each pair of compounds, Fig. 10, the methoxy-substituted compound consistently shows the higher values of T_{NFN}, T_{NFI} and T_{NI}. For each of the transitions, the larger methylthio group contributes to a larger reduction in shape anisotropy and accounts in part for the lower transition temperatures, Fig. 11. In addition, the calculated dipole moment of each On compound is higher than that of the corresponding Sn material. The sterically bulkier methylthio group presumably inhibits the ability of the compounds to pack together in the parallel manner found in the N_F phase.⁶³ The observation of the N_X phase for S1 and S7 may simply reflect the greater suppression of the N_F phase by the methylthio group revealing the underlying N_X phase rather than from any specific stabilising effect. The generality of these observations now requires further investigation.



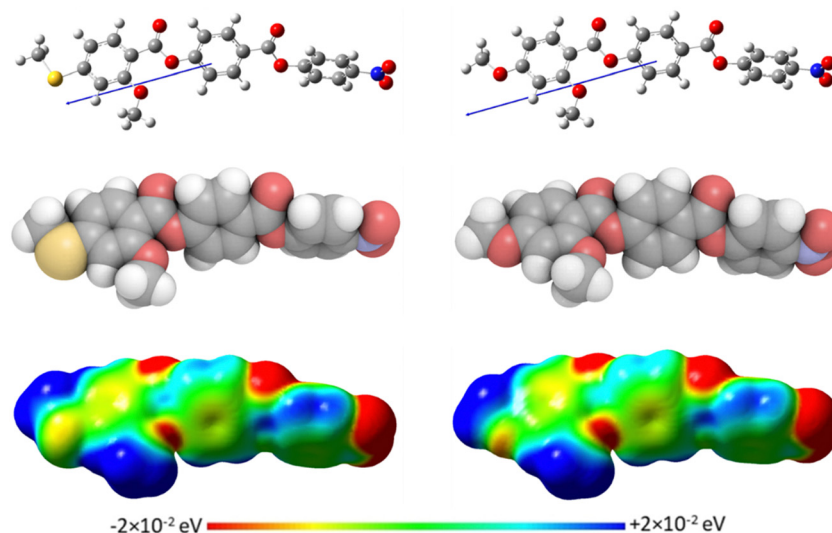


Fig. 11 Molecular modelling of: **S1** (left) and **O1** (right) calculated at the B3LYP/6-31(d) level of theory. The molecules are visualized using: (top) ball and stick models, (middle) space-filling models and (bottom) electrostatic potential surfaces. The arrow indicates the direction of the calculated dipole moment, with the head representing positive charge moving to the base which is negative.

We recently reported the properties of the ethyl substituted compound, 2EC6F (Fig. 12), corresponding to **S8** and **O8**. 2EC6F exhibits a N_F -I transition at 132 °C.⁹ This implies that the decrease in T_{NI} on replacing the methoxy group by an ethyl group is at least 25 K and for the methylthio group at least 11 K. By contrast, the value of T_{NFI} is just 10 K lower than T_{NFN} of **O8** and 8 K higher than that of **S8**. At first sight the reduction in T_{NI} between **S8** and 2EC6F is surprising given that the ethyl group is more compact than the methylthio unit. We have shown, however, for other low molar mass systems that the values of T_{NI} for systems containing methylthio and ethylthio terminal groups are higher than expected based on the behaviour of longer chain homologues, and attributed this to a specific interaction between the molecules, possibly a chalcogen bond.²⁸ This would also account for the surprisingly high T_{NI} seen for **S8** but this interaction appears not to stabilise the N_F phase. Instead, the ethyl group is a better electron donating group than methylthio, and this decreases the amplitude of the charge density at the end of the molecule stabilising the N_F phase. This also accounts for the more stable N_F phase shown by **O8** given that the methoxy group is also a stronger electron donating group. In addition, in terms of molecule shape, the methoxy unit lies in the plane of the phenyl ring to which it is attached, whereas the ethyl group protrudes at an angle disrupting the formation of the N_F phase.

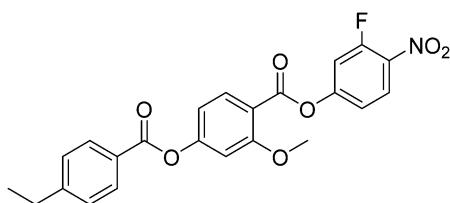


Fig. 12 Molecular structure of 2EC6F.

Conclusions

We have reported the first set of ferroelectric nematogens containing a sulfur atom, **S1–8**, specifically in the form of a methylthio group, and compared their properties to those of the corresponding materials containing a methoxy group, **O1–8**. The difference in the transition temperatures within the S_n and O_n series may be accounted for in terms of the change in shape and electronic properties, based on the extent of fluorination along the molecular backbone. The behaviour of these materials can be accounted for within the framework of a molecular model developed by Madhusudana.⁶³

The molecular dipole moment alone, however, is not necessarily a good indicator of the stability of the N_F phase, with compounds possessing higher dipole moments exhibiting transitions to the N_F phase at lower temperatures. On comparing the properties of corresponding members of the two sets of materials, the methoxy-substituted compound consistently shows the higher values of T_{NFN} , T_{NFI} and T_{NI} . This is attributed to the larger reduction in molecular shape anisotropy associated with the methylthio group and its greater steric bulk. Evidently, the replacement of the terminal methoxy group by the methylthio group did not see a stabilisation of the N_F phase, however, the N_X phase was only observed for two compounds and both of which contained a terminal methylthio group. This may simply reflect the greater suppression of the N_F phase by the methylthio group revealing the underlying N_X phase rather than from any specific stabilising effect. A comparison using the reported behaviour of the ethyl substituted compound corresponding to **S8** and **O8** suggested that the interactions we have reported on previously,²⁸ in terms of methylthio terminated low molar mass mesogens, do not appear to stabilise the N_F phase, as they do for the conventional nematic phase, and this reinforces the view that molecular shape is an important factor in promoting the N_F phase.



Conflicts of interest

There are no conflicts of interest to declare.

Acknowledgements

C.T.I. and J.M.D.S. acknowledge the financial support of the Engineering and Physical Sciences Research Council [EP/V048775/1]. The research was supported by the National Science Centre (Poland) under the grant no. 2021/43/B/ST5/00240.

References

- R. J. Mandle, S. J. Cowling and J. W. Goodby, A nematic to nematic transformation exhibited by a rod-like liquid crystal, *Phys. Chem. Chem. Phys.*, 2017, **19**, 11429–11435.
- H. Nishikawa, K. Shiroshita, H. Higuchi, Y. Okumura, Y. Haseba, S. I. Yamamoto, K. Sago and H. Kikuchi, A Fluid Liquid-Crystal Material with Highly Polar Order, *Adv. Mater.*, 2017, **29**, 1702354.
- R. J. Mandle, S. J. Cowling and J. W. Goodby, Rational Design of Rod-Like Liquid Crystals Exhibiting Two Nematic Phases, *Chem. – A Eur. J.*, 2017, **23**, 14554–14562.
- X. Chen, E. Korblova, D. Dong, X. Wei, R. Shao, L. Radzihovsky, M. A. Glaser, J. E. Maclennan, D. Bedrov, D. M. Walba and N. A. Clark, First-principles experimental demonstration of ferroelectricity in a thermotropic nematic liquid crystal: Polar domains and striking electro-optics, *Proc. Natl. Acad. Sci. U. S. A.*, 2020, **117**, 14021–14031.
- X. Chen, V. Martinez, E. Korblova, G. Freychet, M. Zhernenkov, M. A. Glaser, C. Wang, C. Zhu, L. Radzihovsky, J. E. Maclennan, D. M. Walba and N. A. Clark, The smectic ZA phase: Antiferroelectric smectic order as a prelude to the ferroelectric nematic, *Proc. Natl. Acad. Sci. U. S. A.*, 2022, **120**, e2217150120.
- Y. Song, M. Deng, Z. Wang, J. Li, H. Lei, Z. Wan, R. Xia, S. Aya and M. Huang, Emerging Ferroelectric Uniaxial Lamellar (Smectic AF) Fluids for Bistable In-Plane Polarization Memory, *J. Phys. Chem. Lett.*, 2022, **13**, 9983–9990.
- X. Chen, V. Martinez, P. Nacke, E. Korblova, A. Manabe, M. Klasen-Memmer, G. Freychet, M. Zhernenkov, M. A. Glaser, L. Radzihovsky, J. E. Maclennan, D. M. Walba, M. Bremer, F. Giesselmann, N. A. Clark, N. Abbott and P. Palfy-Muhoray, Observation of a uniaxial ferroelectric smectic A phase, *Proc. Natl. Acad. Sci. U. S. A.*, 2022, **119**, e2210062119.
- S. Brown, E. Cruickshank, J. M. D. Storey, C. T. Imrie, D. Pocięcha, M. Majewska, A. Makal and E. Gorecka, Multiple Polar and Non-polar Nematic Phases, *Chem. Phys. Chem.*, 2021, **22**, 2506–2510.
- E. Cruickshank, P. Rybak, M. M. Majewska, S. Ramsay, C. Wang, C. Zhu, R. Walker, J. M. D. Storey, C. T. Imrie, E. Gorecka and D. Pocięcha, To be or not to be polar: the ferroelectric and antiferroelectric nematic phases, *ACS Omega*, 2023, **8**, 36562–36568.
- J. Li, R. Xia, H. Xu, J. Yang, X. Zhang, J. Kougo, H. Lei, S. Dai, H. Huang, G. Zhang, F. Cen, Y. Jiang, S. Aya and M. Huang, How Far Can We Push the Rigid Oligomers/Polymers toward Ferroelectric Nematic Liquid Crystals?, *J. Am. Chem. Soc.*, 2021, **143**, 46.
- S. Dai, J. Li, J. Kougo, H. Lei, S. Aya and M. Huang, Polar Liquid Crystalline Polymers Bearing Mesogenic Side Chains with Large Dipole Moment, *Macromolecules*, 2021, **54**, 6045–6051.
- D. Pocięcha, R. Walker, E. Cruickshank, J. Szydłowska, P. Rybak, A. Makal, J. Matraszek, J. M. Wolska, J. M. D. Storey, C. T. Imrie and E. Gorecka, Intrinsically chiral ferronematic liquid crystals: an inversion of the helical twist sense at the chiral nematic – chiral ferronematic phase transition, *J. Mol. Liq.*, 2021, **361**, 119532.
- J. Li, H. Nishikawa, J. Kougo, J. Zhou, S. Dai, W. Tang, X. Zhao, Y. Hisai, M. Huang and S. Aya, Development of ferroelectric nematic fluids with giant-dielectricity and non-linear optical properties, *Sci. Adv.*, 2021, **7**, eabf5047.
- J. Li, Z. Wang, M. Deng, Y. Zhu, X. Zhang, R. Xia, Y. Song, Y. Hisai, S. Aya and M. Huang, General Phase-structure Relationship in Polar Rod-shaped Liquid Crystals: Importance of Shape Anisotropy and Dipolar Strength, *Giant*, 2022, **11**, 100109.
- R. Saha, P. Nepal, C. Feng, M. S. Hossain, M. Fukuto, R. Li, J. T. Gleeson, S. Sprunt, R. J. Twieg and A. Jákli, Multiple ferroelectric nematic phases of a highly polar liquid crystal compound, *Liq. Cryst.*, 2022, **49**, 1784–1796.
- A. Manabe, M. Bremer and M. Kraska, Ferroelectric nematic phase at and below room temperature, *Liq. Cryst.*, 2021, **48**, 1079–1086.
- N. Sebastián, R. J. Mandle, A. Petelin, A. Eremin and A. Mertelj, Electrooptics of mm-scale polar domains in the ferroelectric nematic phase, *Liq. Cryst.*, 2021, **48**, 2055–2071.
- N. Tufaha, E. Cruickshank, D. Pocięcha, E. Gorecka, J. M. D. Storey and C. T. Imrie, Molecular Shape, Electronic Factors and the Ferroelectric Nematic Phase, *Chem. – A Eur. J.*, 2023, **29**, e202300073.
- J. Zhou, R. Xia, M. Huang and S. Aya, Stereoisomer effect on ferroelectric nematics: stabilization and phase behavior diversification, *J. Mater. Chem. C*, 2022, **10**, 8762–8766.
- E. Cruickshank, R. Walker, J. M. D. Storey and C. T. Imrie, The effect of a lateral alkyloxy chain on the ferroelectric nematic phase, *RSC Adv.*, 2022, **12**, 29482–29490.
- H. Kikuchi, H. Matsukizono, K. Iwamatsu, S. Endo, S. Anan and Y. Okumura, Fluid Layered Ferroelectrics with Global $C_{\infty v}$ Symmetry, *Adv. Sci.*, 2022, **9**, 2202048.
- R. J. Mandle, A new order of liquids: polar order in nematic liquid crystals, *Soft Matter*, 2022, **18**, 5014–5020.
- N. Sebastián, M. Čopič and A. Mertelj, Ferroelectric nematic liquid-crystalline phases, *Phys. Rev. E*, 2022, **106**, 021001.
- Y. Song, J. Li, R. Xia, H. Xu, X. Zhang, H. Lei, W. Peng, S. Dai, S. Aya and M. Huang, Development of emergent ferroelectric nematic liquid crystals with highly fluorinated and rigid mesogens, *Phys. Chem. Chem. Phys.*, 2022, **24**, 11536–11543.
- E. Cruickshank, A. Pearson, S. Brown, J. M. D. Storey, C. T. Imrie and R. Walker, The ferroelectric nematic phase:



- on the role of lateral alkyloxy chains, *Liq. Cryst.*, 2023, DOI: [10.1080/02678292.2023.2221651](https://doi.org/10.1080/02678292.2023.2221651).
- 26 R. Berardi, M. Ricci and C. Zannoni, Ferroelectric nematic and smectic liquid crystals from tapered molecules, *Chem-PhysChem*, 2001, **2**, 443–447.
 - 27 R. J. Mandle, Supramolecular ferroelectric nematic materials, *Liq. Cryst.*, 2022, **49**, 2019–2026.
 - 28 E. Cruickshank, G. J. Strachan, J. M. D. Storey and C. T. Imrie, Chalcogen bonding and liquid crystallinity: Understanding the anomalous behaviour of the 4'-(alkylthio)[1,1'-biphenyl]-4-carbonitriles (nSCB), *J. Mol. Liq.*, 2021, **346**, 117094.
 - 29 Y. Arakawa, S. Inui and H. Tsuji, Synthesis, phase transitions, and liquid crystal behavior of alkylthio azobenzenes, *Tetrahedron*, 2022, **122**, 132958.
 - 30 Y. Arakawa, S. Inui, K. Igawa and H. Tsuji, Alkylthio- and alkyl-substituted asymmetric diphenyldiacetylene-based liquid crystals: phase transitions, mesophase and single-crystal structures, and birefringence, *Liq. Cryst.*, 2019, **46**, 1621–1630.
 - 31 Y. Arakawa, Y. Ishida, Y. Sasaki, S. Sasaki, M. Tokita and H. Tsuji, Alkylthio-based asymmetric liquid crystals: unravelling the substituent effects and intercalated cybotactic nematic and smectic phases, *Mater. Adv.*, 2022, **3**, 3218–3228.
 - 32 M. Alaasar, A. F. Darweesh, X. Cai, F. Liu and C. Tschierske, Mirror Symmetry Breaking and Network Formation in Achiral Polycatenars with Thioether Tail, *Chem. – A Eur. J.*, 2021, **27**, 14921–14930.
 - 33 Y. Arakawa, S. Kang, J. Watanabe and G. I. Konishi, Assembly of thioether-containing rod-like liquid crystalline materials assisted by hydrogen-bonding terminal carboxyl groups, *RSC Adv.*, 2015, **5**, 8056–8062.
 - 34 E. Cruickshank, G. J. Strachan, M. M. Majewska, D. Pocięcha, E. Górecka, J. M. D. Storey and C. T. Imrie, The effects of alkylthio chains on the properties of symmetric liquid crystal dimers, *New J. Chem.*, 2023, **47**, 7356–7368.
 - 35 E. Cruickshank, M. Salamończyk, D. Pocięcha, G. J. Strachan, J. M. D. Storey, C. Wang, J. Feng, C. Zhu, E. Gorecka and C. T. Imrie, Sulfur-linked cyanobiphenyl-based liquid crystal dimers and the twist-bend nematic phase, *Liq. Cryst.*, 2019, **46**, 1595–1609.
 - 36 Y. Arakawa, K. Komatsu and H. Tsuji, Twist-bend nematic liquid crystals based on thioether linkage, *New J. Chem.*, 2019, **43**, 6786–6793.
 - 37 K. Isoda, T. Ichikawa, K. Kaneko, M. Kondo, T. Sakurai, A. Seki, M. Hara, G. Watanabe, Y. Arakawa, Y. Arai, K. Horita, K. Komatsu and H. Tsuji, Twist-Bend Nematic Phase Behavior of Cyanobiphenyl-Based Dimers with Propane, Ethoxy, and Ethylthio Spacers, *Crystals*, 2022, **12**, 1734.
 - 38 Y. Arakawa, K. Komatsu, Y. Ishida, T. Shiba and H. Tsuji, Thioether-Linked Liquid Crystal Trimers: Odd–Even Effects of Spacers and the Influence of Thioether Bonds on Phase Behavior, *Materials*, 2022, **15**, 1709.
 - 39 Y. Arakawa, K. Komatsu, S. Inui and H. Tsuji, Thioether-linked liquid crystal dimers and trimers: The twist-bend nematic phase, *J. Mol. Struct.*, 2020, **1199**, 126913.
 - 40 Y. Arakawa, K. Komatsu, T. Shiba and H. Tsuji, Methylene- and thioether-linked cyanobiphenyl liquid crystal dimers CBn SCB exhibiting room temperature twist-bend nematic phases and glasses, *Mater. Adv.*, 2021, **2**, 1760–1773.
 - 41 A. J. Seed, K. J. Toyne and J. W. Goodby, Synthesis of some 2,4- and 2,5-disubstituted thiophene systems and the effect of the pattern of substitution on the refractive indices, optical anisotropies, polarisabilities and order parameters in comparison with those of the parent biphenyl and dithien, *J. Mater. Chem.*, 1995, **5**, 653–661.
 - 42 A. Seed, Synthesis of self-organizing mesogenic materials containing a sulfur-based five-membered heterocyclic core, *Chem. Soc. Rev.*, 2007, **36**, 2046–2069.
 - 43 M. K. Reddy, K. S. Reddy, M. Prakash and T. Narasimhaswamy, Synthesis and Characterization of Two Phenyl Ring Core-Based Thiophene Mesogens, *Mol. Cryst. Liq. Cryst.*, 2013, **582**, 1–14.
 - 44 Y. Arakawa, S. Kang, S. Nakajima, K. Sakajiri, S. Kawachi, J. Watanabe and G. Konishi, Synthesis of new wide nematic diaryl-diacetylenes containing thiophene-based heteromonocyclic and heterobicyclic structures, and their birefringence properties, *Liq. Cryst.*, 2014, **41**, 642–651.
 - 45 M. Hird, A. J. Seed, K. J. Toyne, J. W. Goodby, G. W. Gray and D. G. McDonnell, Synthesis, transition temperatures and optical anisotropy of some isothiocyanato-substituted biphenyls, *J. Mater. Chem.*, 1993, **3**, 851–859.
 - 46 G. J. Cross, A. J. Seed, K. J. Toyne, J. W. Goodby, M. Hird and M. C. Artal, Synthesis, transition temperatures, and optical properties of compounds with simple phenyl units linked by double bond, triple bond, ester or propiolate linkages, *J. Mater. Chem.*, 2000, **10**, 1555–1563.
 - 47 A. J. Seed, K. J. Toyne, J. W. Goodby and D. G. McDonnell, Synthesis, optical anisotropies, polarisabilities and order parameters of 4-cyanophenyl and 4-isothiocyanatophenyl 4'-butylsulfanylbenzoates with oxygen and sulfur substitution in the ester linkage, *J. Mater. Chem.*, 1995, **5**, 1–11.
 - 48 Z. Fang and C. Wu, Investigation on thermal behaviour and optical properties of non-symmetric cholesterol-based twin liquid crystals with thioester linkages, *Liq. Cryst.*, 2020, **47**, 1086–1099.
 - 49 Y. Arakawa, Y. Sasaki, N. Haraguchi, S. Itsuno and H. Tsuji, Synthesis, phase transitions and birefringence of novel liquid crystalline 1,4-phenylene bis(4-alkylthio benzoates) and insights into the cybotactic nematic behaviour, *Liq. Cryst.*, 2018, **45**, 821–830.
 - 50 Y. Arakawa and H. Tsuji, Phase transitions and birefringence of bistolane-based nematic molecules with an alkyl, alkoxy and alkylthio group, *Mol. Cryst. Liq. Cryst.*, 2017, **647**, 422–429.
 - 51 Y. Arakawa and H. Tsuji, Selenium-linked liquid crystal dimers for twist-bend nematogens, *J. Mol. Liq.*, 2019, **289**, 111097.
 - 52 Y. Arakawa, H. Kuwahara, M. Tokita and G. Konishi, ichi & Tsuji, H. New fabrication approach to develop a high birefringence photo-crosslinked film based on a sulfur-containing liquid crystalline molecule with large temperature dependence of birefringence, *Mol. Cryst. Liq. Cryst.*, 2018, **662**, 197–207.
 - 53 H. R. H. R. Stapert, S. Del Valle, E. J. K. Versteegen, B. M. I. Van der Zande, J. Lub and S. Stallinga, Photoreplicated



- Anisotropic Liquid-Crystalline Lenses for Aberration Control and Dual-Layer Readout of Optical Discs, *Adv. Funct. Mater.*, 2003, **13**, 732–738.
- 54 I. M. Syed, S. Kaur, H. E. Milton, D. Mistry, J. Bailey, P. B. Morgan, J. Cliff Jones, H. F. Gleeson, H. E. Milton, P. B. Morgan, J. H. Clamp, H. F. Gleeson, J. C. Jones and H. F. Gleeson, Novel switching mode in a vertically aligned liquid crystal contact lens, *Opt. Express*, 2015, **23**, 9911–9916.
- 55 N. Kawatsuki, A. Yamashita, M. Kondo, T. Matsumoto, T. Shioda, A. Emoto and H. Ono, Photoinduced reorientation and polarization holography in photo-cross-linkable liquid crystalline polymer films with large birefringence, *Polymer*, 2010, **51**, 2849–2856.
- 56 M. J. Frisch, G. W. Trucks, H. B. Schlegel, G. E. Scuseria, M. A. Robb, J. R. Cheeseman, G. Scalmani, V. Barone, B. Mennucci, G. A. Petersson, H. Nakatsuji, M. Caricato, X. Li, H. P. Hratchian, A. F. Izmaylov, J. Bloino, G. Zheng, J. L. Sonnenberg, M. Hada, M. Ehara, K. Toyota, R. Fukuda, J. Hasegawa, M. Ishida, T. Nakajima, Y. Honda, O. Kitao, H. Nakai, T. Vreven, J. A. Montgomery, J. E. Peralta, F. Ogliaro, M. Bearpark, J. J. Heyd, E. Brothers, K. N. Kudin, V. N. Staroverov, R. Kobayashi, J. Normand, K. Raghavachari, A. Rendell, J. C. Burant, S. S. Iyengar, J. Tomasi, M. Cossi, N. Rega, J. M. Millam, M. Klene, J. E. Knox, J. B. Cross, V. Bakken, C. Adamo, J. Jaramillo, R. Gomperts, R. E. Stratmann, O. Yazyev, A. J. Austin, R. Cammi, C. Pomelli, J. W. Ochterski, R. L. Martin, K. Morokuma, V. G. Zakrzewski, G. A. Voth, P. Salvador, J. J. Dannenberg, S. Dapprich, A. D. Daniels, J. B. Farkas, Foresman, J. V. Ortiz, J. Cioslowski and D. J. Fox, *Gaussian 09, Revision B.01*, Gaussian, Inc., Wallingford CT. (2010).
- 57 M. Tarini, P. Cignoni and C. Montani, Ambient occlusion and edge cueing to enhance real time molecular visualization, *IEEE Trans. Vis. Comput. Graph.*, 2006, **12**, 1237–1244.
- 58 H. Nishikawa, K. Sano, S. Kurihara, G. Watanabe, A. Nihonyanagi, B. Dhara and F. Araoka, Nano-clustering mediates phase transitions in a diastereomerically-stabilized ferroelectric nematic system, *Commun. Mater.*, 2022, **3**, 89.
- 59 H. Nishikawa, K. Sano and F. Araoka, Anisotropic fluid with phototunable dielectric permittivity, *Nat. Commun.*, 2022, **13**, 1142.
- 60 X. Zhao, J. Zhou, J. Li, J. Kougo, Z. Wan, M. Huang and S. Aya, Spontaneous helielectric nematic liquid crystals: Electric analog to helimagnets, *Proc. Natl. Acad. Sci. U. S. A.*, 2021, **118**, e2111101118.
- 61 A. Erkoreka, J. Martinez-Perdiguero, R. J. Mandle, A. Mertelj and N. Sebastián, Dielectric spectroscopy of a ferroelectric nematic liquid crystal and the effect of the sample thickness, *J. Mol. Liq.*, 2023, **387**, 122566.
- 62 X. Chen, Z. Zhu, M. J. Magrini, E. Korblova, C. S. Park, M. A. Glaser, J. E. Maclennan, D. M. Walba and N. A. Clark, Ideal mixing of paraelectric and ferroelectric nematic phases in liquid crystals of distinct molecular species, *Liq. Cryst.*, 2022, **49**, 1531–1544.
- 63 N. V. Madhusudana, Simple molecular model for ferroelectric nematic liquid crystals exhibited by small rodlike mesogens, *Phys. Rev. E*, 2021, **104**, 014704.



Ferroelectric nematogens containing a methylthio group

¹Gytis Stepanafas, ¹Ewan Cruickshank^{‡,*}, ¹Stevie Brown, ²Magdalena M. Majewska, ²Damian Pociecha, ²Ewa Gorecka, ¹John M.D. Storey & ¹Corrie T. Imrie

¹Department of Chemistry, University of Aberdeen, Old Aberdeen, AB24 3UE, U.K.

[‡]Present Address: School of Pharmacy and Life Sciences, Robert Gordon University, Aberdeen, AB10 7GJ, U.K.

²Faculty of Chemistry, University of Warsaw, ul. Zwirki i Wigury 101, 02-089, Warsaw, Poland

*Author for correspondence: ewan.cruickshank2@abdn.ac.uk

Experimental Procedures

Synthesis

Reagents

All reagents and solvents that were available commercially were purchased from Sigma Aldrich, Fisher Scientific or Fluorochem and were used without further purification unless otherwise stated.

Thin Layer Chromatography

Reactions were monitored using thin layer chromatography, and the appropriate solvent system, using aluminium-backed plates with a coating of Merck Kieselgel 60 F254 silica which were purchased from Merck KGaA. The spots on the plate were visualised by UV light (254 nm) or by oxidation using either a potassium permanganate stain or iodine dip.

Column Chromatography

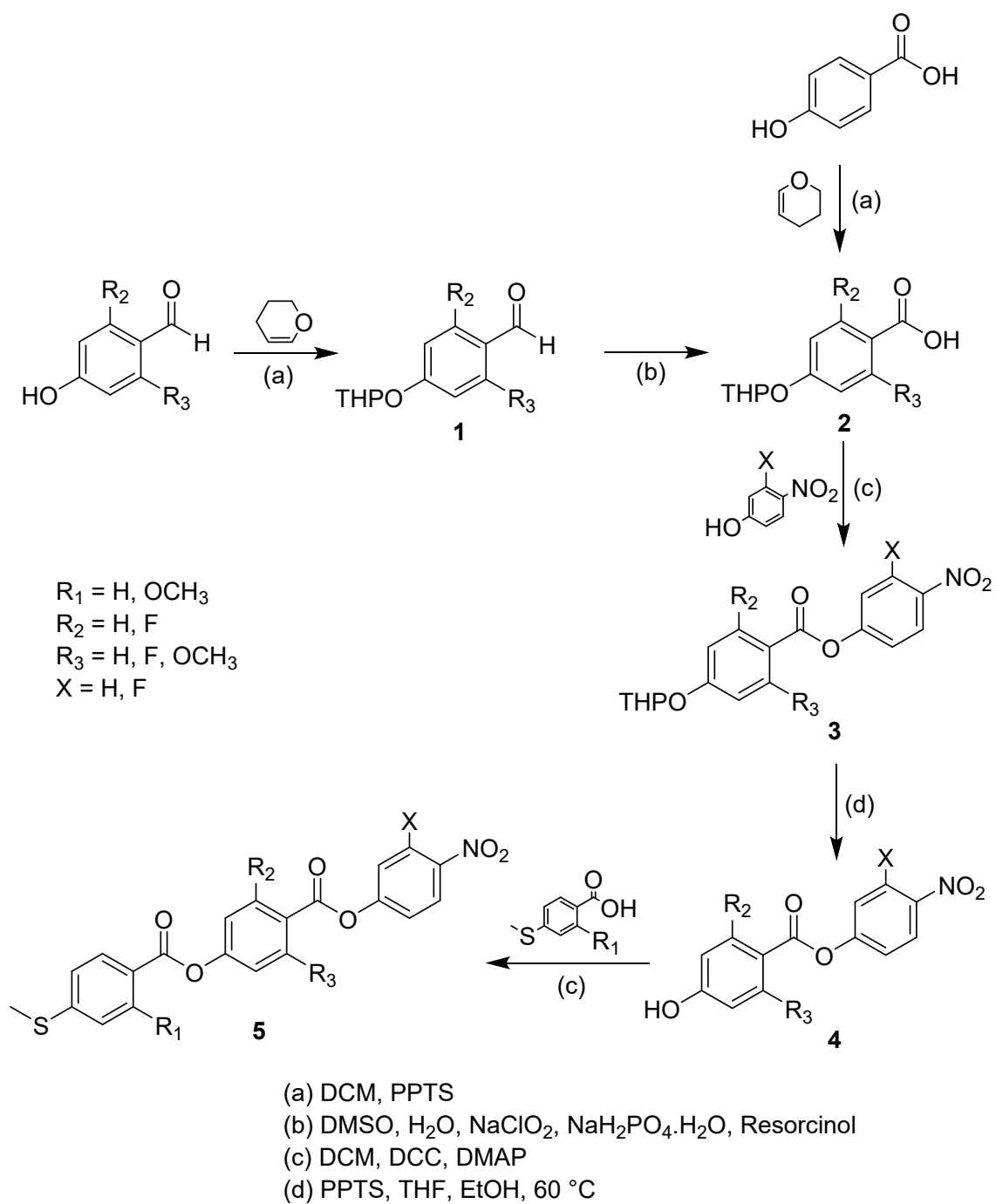
For normal phase column chromatography, the separations were carried out using silica gel grade 60 Å, 40-63 µm particle size, purchased from Fluorochem and using an appropriate solvent system.

Structure Characterisation

All final products and intermediates that were synthesised were characterised using ¹H NMR, ¹³C NMR and infrared spectroscopies. The NMR spectra were recorded on a 400 MHz Bruker Avance III HD NMR spectrometer. The infrared spectra were recorded on a Perkin Elmer Spectrum Two FTIR spectrometer with an ATR diamond cell.

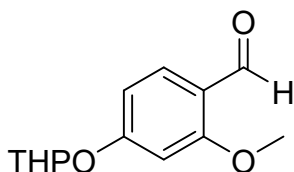
Purity Analysis

In order to determine the purity of the final products, high-resolution mass spectrometry was carried out using a Waters XEVO G2 QToF mass spectrometer by Dr. Morag Douglas at the University of Aberdeen.



Scheme 1. Synthetic route used to obtain the S compounds.

2-Methoxy-4-((tetrahydro-2H-pyran-2-yl)oxy)benzaldehyde (**1a**)



To a pre-dried two-necked round bottom flask, 4-hydroxy-2-methoxy benzaldehyde (5.00 g, 3.30×10^{-2} mol) and pyridinium p-toluenesulfonate (0.828 g, 3.30×10^{-3} mol) were solubilised in dichloromethane, DCM, (100 mL) and the atmosphere was replaced by argon. Then 3,4-dihydro-2H-pyran (3.64 mL, 3.32 g, 3.95×10^{-2} mol) was added through a septum via a syringe and the reaction mixture was left stirring at room temperature for 4 h. The extent of the reaction was monitored by TLC. The mixture was diluted with saturated NaHCO_3 and extracted with DCM. The combined organic extracts were washed with brine, dried over MgSO_4 , the solvent evaporated under vacuum and dry-loaded onto silica gel column for purification using 20% ethyl acetate and 80% petroleum ether (40-60) as the eluent to obtain a colourless oil.

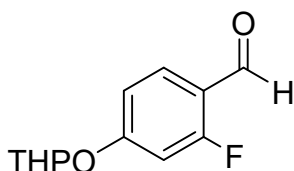
Yield: 5.53 g, 73.6 %. RF: 0.45

IR ($\nu_{\text{max}}/\text{cm}^{-1}$): 2943 (C-H), 1731 (C=O).

^1H NMR (400 MHz, DMSO) δ : 10.19 (d, $J = 0.7$ Hz, 1H, -CHO), 7.66 (d, $J = 8.6$ Hz, 1H, Ar), 6.77 (d, $J = 2.1$ Hz, 1H, Ar), 6.73 (ddd, $J = 8.7, 2.2, 0.8$ Hz, 1H, Ar), 5.67 (t, $J = 3.1$ Hz, 1H, THP), 3.89 (s, 3H, -OCH₃), 3.78 – 3.55 (m, 2H, THP), 1.96 – 1.35 (m, 6H, THP).

^{13}C NMR (101 MHz, DMSO) δ : 187.33, 163.33, 163.23, 129.68, 118.70, 108.41, 100.35, 95.59, 61.62, 55.94, 29.49, 24.54, 18.26.

2-Fluoro-4-((tetrahydro-2H-pyran-2-yl)oxy)benzaldehyde (**1b**)



Quantities used: 2-fluoro-4-hydroxybenzaldehyde (4.50 g, 3.21×10^{-2} mol), 3,4-dihydro-2H-pyran (3.51 mL, 3.24 g, 3.86×10^{-2} mol), PPTS (0.807 g, 3.21×10^{-3} mol), DCM (100 mL). The experimental procedure was described in the preparation of compound **1a**. Column chromatography over silica with DCM as the eluent to obtain white solid.

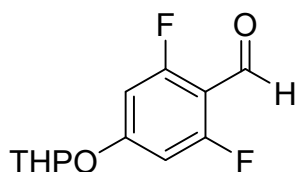
Yield: 5.03 g, 69.4 %. RF: 0.45. Melting Point: 99 °C

IR ($\nu_{\text{max}}/\text{cm}^{-1}$): 3077 (C-H), 2772 ((C=O)-H), 1680 (C=O).

^1H NMR (400 MHz, DMSO) δ : 10.08 (s, 1H, -CHO), 7.79 (t, $J = 8.7$ Hz, 1H, Ar), 7.07 – 6.98 (m, 2H, Ar), 5.68 (t, $J = 3.1$ Hz, 1H, THP), 3.75 – 3.56 (m, 2H, THP), 1.94 – 1.48 (m, 6H, THP).

^{13}C NMR (101 MHz, CDCl_3) δ : 186.26, 186.20, 167.53, 164.97, 163.88, 163.76, 130.06, 130.02, 118.51, 118.43, 113.29, 113.26, 104.01, 103.77, 96.66, 62.19, 30.00, 25.04, 18.36.

2,6-Difluoro-4-((tetrahydro-2H-pyran-2-yl)oxy)benzaldehyde (**1c**)



Quantities used: 2,6-difluoro-4-hydroxybenzaldehyde (5.00 g, 0.032 mol), 3,4-dihydro-2H-pyran (3.46 mL, 3.19 g, 3.80×10^{-2} mol), PPTS (0.794 g, 3.20×10^{-3} mol), DCM (100 mL). The experimental procedure was described in the preparation of compound **1a**. Column chromatography over silica with 20% ethyl acetate and 80% petroleum ether (40-60) as eluent to obtain a colourless oil.

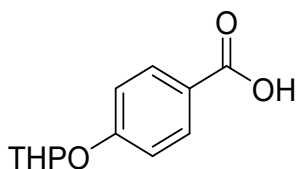
Yield: 4.93 g, 64.1 %. RF: 0.48

IR ($\nu_{\max}/\text{cm}^{-1}$): 3075 (C-H), 1691 (C=O).

^1H NMR (400 MHz, DMSO) δ : 10.07 (s, 1H, -CHO), 6.95 – 6.88 (m, 2H, Ar), 5.72 (t, $J = 2.9$ Hz, 1H, THP), 3.73 – 3.56 (m, 2H, THP), 1.91 – 1.70 (m, 3H, THP), 1.67 – 1.48 (m, 3H, THP).

^{13}C NMR (101 MHz, DMSO) δ : 183.12, 183.07, 183.03, 165.38, 165.28, 165.22, 165.06, 162.81, 162.72, 100.10, 100.08, 100.04, 99.89, 99.85, 99.84, 93.24, 61.65, 30.12, 25.01, 19.13.

4-((Tetrahydro-2H-pyran-2-yl)oxy)benzoic acid (**2a**)



Quantities used: 4-hydroxybenzoic acid (10.0 g, 7.20×10^{-2} mol), 3,4-dihydro-2H-pyran (7.95 mL, 7.31 g, 8.70×10^{-2} mol), PPTS (1.81 g, 7.20×10^{-3} mol), DCM (150 mL). The experimental procedure was described in the preparation of compound **1a**. Column chromatography over silica with 20:80 ethyl acetate and petroleum ether (40-60) as the eluent followed by recrystallisation from ethanol (100 mL) to obtain white solid.

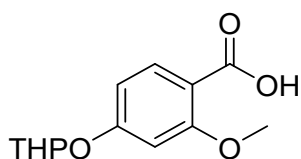
Yield: 5.08 g, 31.1 %. RF: 0.30. Melting Point: 170 °C

IR ($\nu_{\max}/\text{cm}^{-1}$): 3071-2946 (OH), 1668 (C=O).

^1H NMR (400 MHz, DMSO) δ : 12.64 (s, 1H, -COOH), 7.88 (d, $J = 8.6$ Hz, 2H, Ar), 7.09 (d, $J = 9.0$ Hz, 2H, Ar), 5.58 (t, $J = 3.2$ Hz, 1H, THP), 3.72 (ddd, $J = 12.1, 8.9, 3.5$ Hz, 1H, THP), 3.57 (dt, $J = 10.8, 4.4$ Hz, 1H, THP), 1.95 – 1.69 (m, 3H, THP), 1.69 – 1.46 (m, 3H, THP).

^{13}C NMR (101 MHz, DMSO) δ : 166.96, 160.14, 131.20, 123.76, 115.94, 95.57, 61.66, 29.66, 24.59, 18.47.

2-Methoxy-4-((tetrahydro-2H-pyran-2-yl)oxy)benzoic acid (**2b**)



To a round bottom flask, compound **1a** (2.78 g, 1.20×10^{-2} mol) and resorcinol (1.94 g, 1.80×10^{-2} mol) were dissolved in DMSO (50 mL). Sodium chlorite (4.32 g, 4.80×10^{-2} mol) and sodium dihydrogen phosphate monohydrate (5.80 g, 4.20×10^{-2} mol) were dissolved in water (40 mL) and slowly added to a stirred solution of aldehyde **1a** with cooling by ice-water. The mixture was allowed to warm to room temperature and stirred for 6 hours. The reaction was monitored by TLC using 80:20 mix of ethyl acetate and petroleum ether (40-60). The mixture was diluted with water and solid NaHCO_3 was added to adjust the solution pH to 8. The mixture was washed with ethyl acetate, then the pH was adjusted to 4 by the addition of 1M hydrochloric acid and extracted with ethyl acetate. The combined organic extracts were washed with brine and dried over MgSO_4 . The solvent was removed under reduced pressure to give a brown oil.

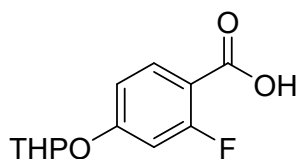
Yield: 1.95 g, 65.7 %. RF: 0.55

IR ($\nu_{\text{max}}/\text{cm}^{-1}$): 3028 (OH), 2949 (C-H), 1695 (C=O).

^1H NMR (400 MHz, DMSO) δ : 11.95 (s, 1H, -COOH), 7.61 (d, $J = 8.5$ Hz, 1H, Ar), 6.45 (d, $J = 2.2$ Hz, 1H, Ar), 6.38 (dd, $J = 8.6, 2.2$ Hz, 1H, Ar), 5.58 (t, $J = 3.1$ Hz, 1H, THP), 3.75 (s, 3H, -OCH₃), 3.62 – 3.40 (m, 2H, THP), 1.94 – 1.35 (m, 6H, THP).

^{13}C NMR (101 MHz, DMSO) δ : 166.44, 162.53, 160.97, 133.57, 110.75, 107.17, 99.49, 97.83, 61.39, 55.49, 30.40, 25.07, 19.30.

2-Fluoro-4-((tetrahydro-2H-pyran-2-yl)oxy)benzoic acid (**2c**)



Quantities used: compound **1b** (4.93 g, 2.20×10^{-2} mol), resorcinol (3.63 g, 3.30×10^{-2} mol), sodium chlorite (7.92 g, 8.80×10^{-2} mol), sodium dihydrogen phosphate monohydrate (10.8 g, 7.70×10^{-2} mol), DMSO (80 mL), water (40 mL). The experimental procedure was described in the preparation of compound **2b**. The reaction mixture was stirred overnight at room temperature and the extent was monitored by TLC using 80:20 mix of petroleum ether (40-60) and ethyl acetate. The mixture was diluted with water and the pH was adjusted to 4 by the addition of 1M HCl solution. The precipitate was removed by vacuum filtration and followed by recrystallisation from ethanol (100 mL) to obtain a pale-yellow solid.

Yield: 3.43 g, 64.9 %. RF: 0.10. Melting Point: 149 °C

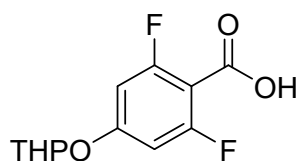
IR ($\nu_{\text{max}}/\text{cm}^{-1}$): 3082 (OH), 1677 (C=O).

^1H NMR (400 MHz, DMSO) δ : 12.89 (s, 1H, -COOH), 7.86 – 7.77 (m, 1H, Ar), 6.97 – 6.89

(m, 2H, Ar), 5.61 (t, $J = 3.1$ Hz, 1H, THP), 3.75 – 3.65 (m, 1H, THP), 3.63 – 3.55 (m, 1H, THP), 1.93 – 1.68 (m, 3H, THP), 1.68 – 1.47 (m, 3H, THP).

^{13}C NMR (101 MHz, CDCl_3) δ : 169.53, 169.50, 165.50, 163.12, 163.00, 162.90, 134.06, 134.04, 112.42, 112.39, 110.58, 110.49, 105.03, 104.78, 96.57, 62.19, 30.03, 25.06, 18.41.

2,6-Difluoro-4-((tetrahydro-2H-pyran-2-yl)oxy)benzoic acid (**2d**)



Quantities used: compound **1c** (4.93 g, 2.00×10^{-2} mol), resorcinol (3.36 g, 3.10×10^{-2} mol), sodium chlorite (7.33 g, 8.10×10^{-2} mol), sodium dihydrogen phosphate monohydrate (9.98 g, 7.10×10^{-2} mol), DMSO (80 mL), water (60 mL). The experimental procedure was described in the preparation of compound **2b**. The reaction mixture was stirred overnight at room temperature and the extent was monitored by TLC using 80:20 mix of petroleum ether (40-60) and ethyl acetate. The mixture was diluted with water and the pH was adjusted to 4 by the addition of 1M HCl solution. The aqueous layer was extracted with ethyl acetate. The combined organic layer was washed with water, brine and dried over MgSO_4 . The solvent was removed to obtain a brown oil.

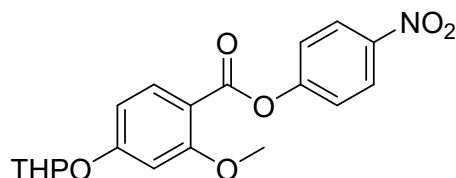
Yield: 3.59 g, 68.3 %. RF: 0.080

IR ($\nu_{\text{max}}/\text{cm}^{-1}$): 3060 (OH), 1687 (C=O).

^1H NMR (400 MHz, DMSO) δ : 13.07 (s, 1H, -COOH), 6.90 – 6.80 (m, 2H, Ar), 5.62 (t, $J = 3.1$ Hz, 1H, THP), 3.74 – 3.55 (m, 2H, THP), 1.91 – 1.68 (m, 3H, THP), 1.67 – 1.46 (m, 3H, THP).

^{13}C NMR (101 MHz, DMSO) δ : 162.72, 162.62, 162.29, 161.78, 161.63, 161.48, 160.22, 160.12, 99.85, 99.82, 99.78, 99.59, 99.57, 93.27, 61.67, 30.14, 25.03, 19.14.

4-Nitrophenyl-2-methoxy-4-((tetrahydro-2H-pyran-2-yl)oxy)benzoate (**3a**)



To a pre-dried flask, compound **2b** (2.77 g, 1.10×10^{-2} mol) was added and dissolved in DCM (50 mL). The addition of *N,N'*-dicyclohexylcarbodiimide, DCC, (2.68 g, 1.30×10^{-2} mol) was followed by 4-nitrophenol (1.39 g, 1.00×10^{-2} mol) and the mixture was allowed to stir for 2 min before adding 4-dimethylaminopyridine, DMAP (0.122 g, 1.00×10^{-3} mol). The reaction mixture was stirred overnight at room temperature and the extent was monitored by TLC. The white precipitate was removed by filtration and the solvent was evaporated under vacuum to

leave crude solid. This was purified using silica chromatography with DCM as the eluent to obtain pale yellow solid.

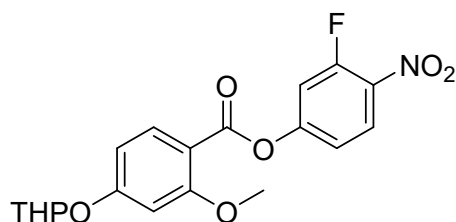
Yield: 1.20 g, 32.1 %. RF: 0.73. Melting Point: 149 °C

IR ($\nu_{\max}/\text{cm}^{-1}$): 2965 (C-H), 1733 (C=O).

^1H NMR (400 MHz, DMSO) δ : 8.33 (d, $J = 9.1$ Hz, 2H, Ar), 7.98 (d, $J = 8.7$ Hz, 1H, Ar), 7.53 (d, $J = 8.9$ Hz, 2H, Ar), 6.81 (d, $J = 2.2$ Hz, 1H, Ar), 6.78 (dd, $J = 8.7, 2.2$ Hz, 1H, Ar), 5.69 (t, $J = 3.1$ Hz, 1H, THP), 3.86 (s, 3H, -OCH₃), 3.75 (ddd, $J = 12.4, 9.3, 3.5$ Hz, 1H, THP), 3.61 (dt, $J = 11.0, 4.3$ Hz, 1H, THP), 1.96 – 1.72 (m, 4H, THP), 1.70 – 1.52 (m, 2H, THP).

^{13}C NMR (101 MHz, DMSO) δ : 162.42, 162.09, 161.71, 155.80, 144.89, 134.04, 125.25, 123.41, 110.17, 107.75, 101.11, 95.62, 61.61, 56.05, 29.52, 24.56, 18.28.

3-Fluoro-4-nitrophenyl 2-methoxy-4-((tetrahydro-2H-pyran-2-yl)oxy)benzoate (**3b**)



Quantities used: compound **2b** (5.15 g, 2.00×10^{-2} mol), 3-fluoro-4-nitrophenol (2.92 g, 1.90×10^{-2} mol), DCC (4.96 g, 2.40×10^{-2} mol), DMAP (0.227 g, 1.86×10^{-3} mol), DCM (100 mL). The experimental procedure was described in preparation of compound **3a**. Column chromatography over silica with DCM as the eluent followed by recrystallisation from ethanol (100 mL) to obtain a pale yellow solid.

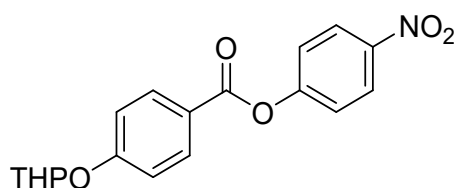
Yield: 3.36 g, 46.2 %. RF: 0.43. Melting Point: 115 °C

IR ($\nu_{\max}/\text{cm}^{-1}$): 3112 (C-H), 1700 (C=O).

^1H NMR (400 MHz, DMSO) δ : 8.28 (t, $J = 8.8$ Hz, 1H, Ar), 7.99 (d, $J = 8.8$ Hz, 1H, Ar), 7.67 (dd, $J = 12.2, 2.4$ Hz, 1H, Ar), 7.41 – 7.33 (m, 1H, Ar), 6.84 – 6.74 (m, 2H, Ar), 5.70 (t, $J = 3.1$ Hz, 1H, THP), 3.86 (s, 3H, -OCH₃), 3.79 – 3.57 (m, 2H, THP), 1.99 – 1.47 (m, 6H, THP).

^{13}C NMR (101 MHz, CDCl₃) δ : 163.49, 162.82, 162.04, 157.66, 156.48, 156.37, 155.01, 134.56, 127.14, 127.12, 118.39, 118.35, 112.67, 112.43, 110.01, 107.97, 100.83, 96.38, 62.18, 56.19, 30.15, 25.13, 18.47.

4-Nitrophenyl-4-((tetrahydro-2H-pyran-2-yl)oxy)benzoate (**3c**)



Quantities used: compound **2a** (2.00 g, 9.00×10^{-3} mol), 4-nitrophenol (1.38 g, 9.91×10^{-3} mol), DCC (3.71 g, 1.80×10^{-2} mol), DMAP (0.110 g, 9.00×10^{-4} mol), DCM (100 mL). The experimental procedure was described in preparation of compound **3a**. Column chromatography over silica with DCM as the eluent followed by recrystallisation from ethanol (100 mL) to obtain a white solid.

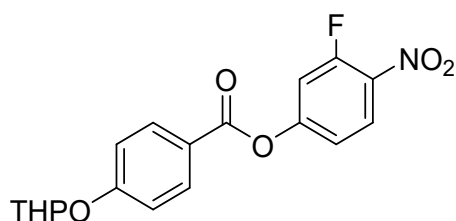
Yield: 2.02 g, 65.1 %. RF: 0.73. Melting Point: 133 °C

IR ($\nu_{\max}/\text{cm}^{-1}$): 2959 (C-H), 1735 (C=O).

^1H NMR (400 MHz, DMSO) δ : 8.35 (d, $J = 9.2$ Hz, 2H, Ar), 8.10 (d, $J = 9.0$ Hz, 2H, Ar), 7.59 (d, $J = 9.3$ Hz, 2H, Ar), 7.22 (d, $J = 9.0$ Hz, 2H, Ar), 5.67 (t, $J = 3.1$ Hz, 1H, THP), 3.78 – 3.67 (m, 1H, THP), 3.64 – 3.55 (m, 1H, THP), 1.97 – 1.72 (m, 3H, THP), 1.72 – 1.49 (m, 3H, THP).

^{13}C NMR (101 MHz, DMSO) δ : 163.48, 161.31, 155.66, 145.05, 132.15, 125.27, 123.36, 121.01, 116.44, 95.56, 61.63, 29.52, 24.53, 18.32.

3-Fluoro-4-nitrophenyl-4-((tetrahydro-2H-pyran-2-yl)oxy)benzoate (**3d**)



Quantities used: compound **2a** (2.00 g, 9.00×10^{-3} mol), 3-fluoro-4-nitrophenol (1.56 g, 9.91×10^{-3} mol), DCC (3.71 g, 1.80×10^{-2} mol), DMAP (0.110 g, 9.00×10^{-4} mol), DCM (100 mL). The experimental procedure was described in preparation of compound **3a**. Column chromatography over silica with DCM as the eluent followed by recrystallisation from ethanol (100 mL) to obtain faint yellow solid.

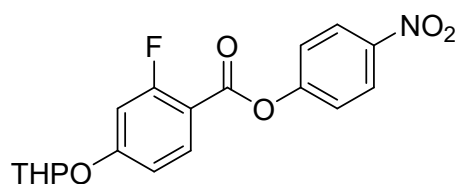
Yield: 1.81 g, 55.6 %. RF: 0.73. Melting Point: 105 °C

IR ($\nu_{\max}/\text{cm}^{-1}$): 2952 (C-H), 1733 (C=O).

^1H NMR (400 MHz, DMSO) δ : 8.30 (t, $J = 8.9$ Hz, 1H, Ar), 8.10 (d, $J = 9.0$ Hz, 2H, Ar), 7.73 (dd, $J = 12.1, 2.4$ Hz, 1H, Ar), 7.44 (ddd, $J = 9.0, 2.4, 1.2$ Hz, 1H, Ar), 7.22 (d, $J = 8.9$ Hz, 2H, Ar), 5.67 (t, $J = 3.1$ Hz, 1H, THP), 3.77 – 3.67 (m, 1H, THP), 3.64 – 3.55 (m, 1H, THP), 1.96 – 1.72 (m, 3H, THP), 1.72 – 1.51 (m, 3H, THP).

^{13}C NMR (101 MHz, DMSO) δ : 163.15, 161.41, 156.55, 155.83, 155.72, 153.93, 134.62, 134.54, 132.23, 127.49, 127.47, 120.72, 119.23, 119.20, 116.47, 112.92, 112.68, 95.57, 61.64, 29.51, 24.52, 18.31.

3-Fluoro-4-nitrophenyl-4-((tetrahydro-2H-pyran-2-yl)oxy)benzoate (**3e**)



Quantities used: compound **2c** (1.63 g, 6.79×10^{-3} mol), 4-nitrophenol (0.858 g, 6.17×10^{-3} mol), DCC (1.65 g, 8.02×10^{-3} mol), DMAP (0.0750 g, 6.17×10^{-4} mol), DCM (50 mL). The experimental procedure was described in preparation of compound **3a**. Column chromatography over silica with DCM as the eluent followed by recrystallisation from ethanol (50 mL) to obtain an off-white solid.

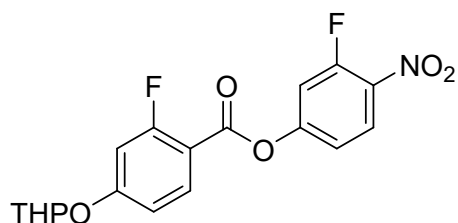
Yield: 1.53 g, 69.0 %. RF: 0.53. Melting Point: 125 °C

IR ($\nu_{\max}/\text{cm}^{-1}$): 3112 (C-H), 1722 (C=O)

^1H NMR (400 MHz, CDCl_3) δ : 8.35 – 8.29 (m, 2H, Ar), 8.04 (t, $J = 8.7$ Hz, 1H, Ar), 7.45 – 7.39 (m, 2H, Ar), 6.97 – 6.88 (m, 2H, Ar), 5.53 (t, $J = 3.0$ Hz, 1H, THP), 3.86 – 3.79 (m, 1H, THP), 3.70 – 3.62 (m, 1H, THP), 2.07 – 1.87 (m, 3H, THP), 1.81 – 1.58 (m, 3H, THP).

^{13}C NMR (101 MHz, DMSO) δ : 164.36, 162.66, 162.54, 161.78, 160.81, 160.77, 155.27, 145.16, 133.80, 133.78, 125.30, 123.39, 112.96, 112.93, 109.41, 109.32, 104.98, 104.73, 95.92, 61.67, 29.29, 24.44, 18.14.

3-Fluoro-4-nitrophenyl 2-fluoro-4-((tetrahydro-2H-pyran-2-yl)oxy)benzoate (**3f**)



Quantities used: compound **2c** (1.63 g, 6.79×10^{-3} mol), 3-fluoro-4-nitrophenol (0.969 g, 6.17×10^{-3} mol), DCC (1.65 g, 8.02×10^{-3} mol), DMAP (0.0750 g, 6.17×10^{-4} mol), DCM (50 mL). The experimental procedure was described in preparation of compound **3a**. Column chromatography over silica with DCM as the eluent followed by recrystallisation from ethanol (50 mL) to obtain an off-white solid.

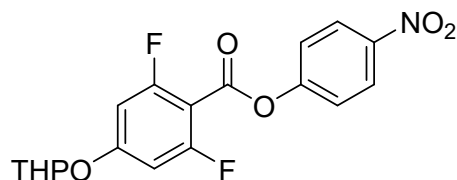
Yield: 1.35 g, 58.1 %. RF: 0.60. Melting Point: 146 °C

IR ($\nu_{\max}/\text{cm}^{-1}$): 3104 (C-H), 1743 (C=O).

^1H NMR (400 MHz, CDCl_3) δ : 8.18 (t, $J = 8.7$ Hz, 1H, Ar), 8.02 (t, $J = 8.7$ Hz, 1H, Ar), 7.29 (dd, $J = 11.3, 2.3$ Hz, 1H, Ar), 7.24 – 7.19 (m, 1H, Ar), 6.97 – 6.88 (m, 2H, Ar), 5.53 (t, $J = 3.0$ Hz, 1H, THP), 3.87 – 3.79 (m, 1H, THP), 3.70 – 3.63 (m, 1H, THP), 2.07 – 1.87 (m, 3H, THP), 1.80 – 1.59 (m, 3H, THP).

^{13}C NMR (101 MHz, DMSO) δ : 164.43, 162.79, 162.67, 161.85, 160.42, 160.37, 156.55, 155.41, 155.30, 153.93, 134.73, 134.66, 133.85, 133.83, 127.52, 127.50, 119.26, 119.22, 112.99, 112.73, 109.13, 109.04, 104.99, 104.74, 95.94, 61.68, 29.28, 24.44, 18.13.

4-Nitrophenyl 2,6-difluoro-4-((tetrahydro-2H-pyran-2-yl)oxy)benzoate (**3g**)



Quantities used: compound **2d** (1.68 g, 6.49×10^{-3} mol), 4-nitrophenol (0.820 g, 5.90×10^{-3} mol), DCC (1.58 g, 7.67×10^{-3} mol), DMAP (0.0720 g, 5.90×10^{-4} mol), DCM (100 mL). The experimental procedure was described in preparation of compound **3a**. Column chromatography over silica with DCM as the eluent followed by recrystallisation from ethanol (20 mL) to obtain a white solid.

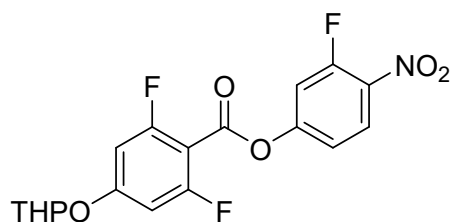
Yield: 0.275 g, 12.3 %. RF: 0.53. Melting Point: 106 °C

IR ($\nu_{\text{max}}/\text{cm}^{-1}$): 3116 (C-H), 1749 (C=O).

^1H NMR (400 MHz, DMSO) δ : 8.38 – 8.33 (m, 2H, Ar), 7.62 – 7.56 (m, 2H, Ar), 7.06 – 6.98 (m, 2H, Ar), 5.74 (t, $J = 2.9$ Hz, 1H, THP), 3.75 – 3.59 (m, 2H, THP), 1.88 – 1.73 (m, 3H, THP), 1.66 – 1.52 (m, 3H, THP).

^{13}C NMR (101 MHz, DMSO) δ : 163.43, 163.35, 161.91, 161.75, 161.60, 160.88, 160.80, 154.73, 145.36, 125.47, 123.25, 101.56, 101.31, 101.28, 96.20, 61.71, 29.08, 24.35, 18.00.

3-Fluoro-4-nitrophenyl 2,6-difluoro-4-((tetrahydro-2H-pyran-2-yl)oxy)benzoate (**3h**)



Quantities used: compound **2d** (1.83 g, 7.09×10^{-3} mol), 3-fluoro-4-nitrophenol (1.01 g, 6.44×10^{-3} mol), DCC (1.73 g, 8.38×10^{-3} mol), DMAP (0.0790 g, 6.44×10^{-4} mol), DCM (100 mL). The experimental procedure was described in preparation of compound **3a**. Column chromatography over silica with DCM as the eluent followed by recrystallisation from ethanol (20 mL) to obtain a white solid.

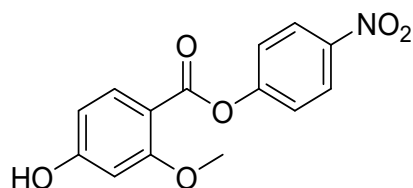
Yield: 0.332 g, 13.1 %. RF: 0.58. Melting Point: 184 °C

IR ($\nu_{\text{max}}/\text{cm}^{-1}$): 3110 (C-H), 1738 (C=O).

^1H NMR (400 MHz, DMSO) δ : 8.31 (t, $J = 8.8$ Hz, 1H, Ar), 7.73 (dd, $J = 11.9, 2.4$ Hz, 1H, Ar), 7.42 (ddd, $J = 9.1, 2.5, 1.2$ Hz, 1H, Ar), 7.06 – 6.98 (m, 2H, Ar), 5.74 (t, $J = 2.9$ Hz, 1H, THP), 3.79 – 3.59 (m, 2H, THP), 1.93 – 1.73 (m, 3H, THP), 1.71 – 1.49 (m, 3H, THP).

^{13}C NMR (101 MHz, DMSO) δ : 163.58, 163.50, 161.95, 161.03, 160.94, 158.03, 156.59, 154.80, 154.69, 153.97, 134.95, 134.88, 127.70, 127.68, 119.10, 119.06, 112.88, 112.64, 101.61, 101.57, 101.35, 101.31, 96.21, 61.72, 29.07, 24.34, 18.56.

4-Nitrophenyl-2-methoxy-4-hydroxybenzoate (**4a**)



A round bottom flask was charged with **3a** (0.620 g, 1.65×10^{-3} mol), pyridinium p-toluenesulfonate (0.0410 g, 1.65×10^{-4} mol), THF (20 mL) and ethanol (20 mL). The solution was heated to 60 °C and stirred for 6 h. The extent of the reaction was monitored by TLC using 95:5 DCM and ethyl acetate as the solvent. Once the reaction was completed, solvent was removed under vacuum and replaced with DCM. The organic layer was washed with water, brine and dried over MgSO_4 . The solvent was removed to obtain off-white solid which was carried forward without further purification.

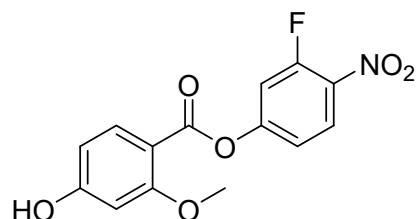
Yield: 0.460 g, 97.2 %. RF: 0.40. Melting Point: 217 °C

IR ($\nu_{\text{max}}/\text{cm}^{-1}$): 3327 (OH), 2940 (C-H), 1699 (C=O).

^1H NMR (400 MHz, DMSO) δ : 10.07 (s, 1H, -OH), 7.82 (d, $J = 9.2$ Hz, 2H, Ar), 7.41 (d, $J = 8.6$ Hz, 1H, Ar), 7.01 (d, $J = 9.2$ Hz, 2H, Ar), 6.05 (d, $J = 2.2$ Hz, 1H, Ar), 6.00 (dd, $J = 8.6, 2.2$ Hz, 1H, Ar), 3.32 (s, 3H, -OCH₃).

^{13}C NMR (101 MHz, DMSO) δ : 164.70, 162.82, 162.52, 156.42, 145.21, 134.92, 125.65, 123.85, 108.20, 100.17, 93.72, 56.19.

3-Fluoro-4-nitrophenyl 4-hydroxy-2-methoxybenzoate (**4b**)



Quantities used: compound **3b** (0.464 g, 1.19×10^{-3} mol), PPTS (0.0300 g, 1.19×10^{-4} mol), ethanol (20 mL), THF (20 mL). The experimental procedure was described in preparation of compound **4a**. Once the reaction was completed, solvent was removed under vacuum and replaced with DCM. The organic layer was washed with water, brine and dried over MgSO_4 . The solvent was removed to obtain off-white solid which was carried forward without further

purification.

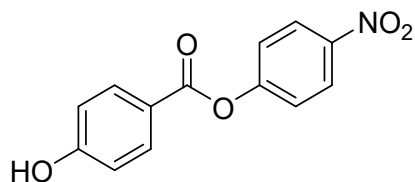
Yield: 0.226 g, 62.1 %. RF: 0.43. Melting Point: 217 °C

IR ($\nu_{\max}/\text{cm}^{-1}$): 3333 (OH), 3062 (C-H), 1702 (C=O).

^1H NMR (400 MHz, DMSO) δ : 10.65 (s, 1H, -OH), 8.26 (t, $J = 8.9$ Hz, 1H, Ar), 7.90 (d, $J = 8.7$ Hz, 1H, Ar), 7.64 (dd, $J = 12.2, 2.4$ Hz, 1H, Ar), 7.38 – 7.31 (m, 1H, Ar), 6.57 – 6.47 (m, 2H, Ar), 3.81 (s, 3H, -OCH₃).

^{13}C NMR (101 MHz, DMSO) δ : 164.49, 162.59, 161.57, 156.66, 156.26, 156.15, 154.05, 134.64, 134.31, 134.24, 127.41, 127.39, 119.31, 119.27, 112.90, 112.67, 107.83, 107.20, 99.75, 55.79.

4-Nitrophenyl-4-hydroxybenzoate (**4c**)



Quantities used: compound **3c** (1.92 g, 5.59×10^{-3} mol), PPTS (0.140 g, 5.59×10^{-4} mol), ethanol (40 mL), THF (40 mL). The experimental procedure was described in preparation of compound **4a**. Once the reaction was completed, solvent was removed under vacuum and replaced with ethyl acetate. The organic layer was washed with water, brine and dried over MgSO₄. The solvent was removed to obtain off-white solid which was carried forward without further purification.

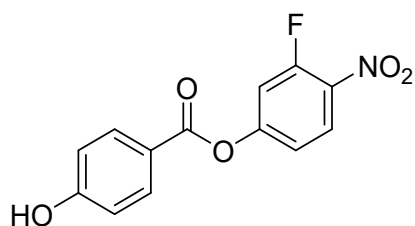
Yield: 1.31 g, 90.3 %. RF: 0.68. Melting Point: 218 °C

IR ($\nu_{\max}/\text{cm}^{-1}$): 3445 (OH), 2989 (C-H), 1733 (C=O).

^1H NMR (400 MHz, DMSO) δ : 10.63 (s, 1H, -OH), 8.33 (d, $J = 9.2$ Hz, 2H, Ar), 8.01 (d, $J = 8.7$ Hz, 2H, Ar), 7.57 (d, $J = 9.3$ Hz, 2H, Ar), 6.95 (d, $J = 8.8$ Hz, 2H, Ar).

^{13}C NMR (101 MHz, DMSO) δ : 163.64, 163.10, 155.79, 144.96, 132.54, 125.25, 123.37, 118.56, 115.73.

3-Fluoro-4-nitrophenyl-4-hydroxybenzoate (**4d**)



Quantities used: compound **3c** (1.71 g, 4.74×10^{-3} mol), PPTS (0.119 g, 4.74×10^{-4} mol), ethanol (40 mL), THF (40 mL). The experimental procedure was described in preparation of compound

4a. Once the reaction was completed, solvent was removed under vacuum and replaced with ethyl acetate. The organic layer was washed with water, brine and dried over MgSO_4 . The solvent was removed to obtain pale yellow solid which was carried forward without further purification.

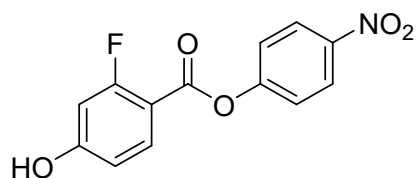
Yield: 1.22 g, 92.5 %. RF: 0.68. Melting Point: 196 °C

IR ($\nu_{\text{max}}/\text{cm}^{-1}$): 3383 (OH), 2956 (C-H), 1708 (C=O).

^1H NMR (400 MHz, DMSO) δ : 10.66 (s, 1H, -OH), 8.28 (t, $J = 8.9$ Hz, 1H, Ar), 8.00 (d, $J = 8.9$ Hz, 2H, Ar), 7.71 (dd, $J = 12.1, 2.4$ Hz, 1H, Ar), 7.41 (ddd, $J = 9.1, 2.4, 1.2$ Hz, 1H, Ar), 6.95 (d, $J = 8.8$ Hz, 2H, Ar).

^{13}C NMR (101 MHz, DMSO) δ : 163.30, 163.24, 156.57, 156.00, 155.89, 153.96, 134.51, 134.43, 132.64, 127.44, 127.42, 119.22, 119.18, 118.27, 115.77, 112.90, 112.66.

4-Nitrophenyl 2-fluoro-4-hydroxybenzoate (**4e**)



Quantities used: compound **3e** (1.44 g, 3.99×10^{-3} mol), PPTS (0.100 g, 3.99×10^{-4} mol), ethanol (30 mL), THF (30 mL). The experimental procedure was described in preparation of compound **4a**. Once the reaction was completed, solvent was removed under vacuum and replaced with ethyl acetate. The organic layer was washed with water, brine and dried over MgSO_4 . The solvent was removed to obtain pale yellow solid which was carried forward without further purification.

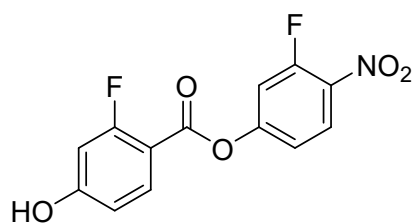
Yield: 1.06 g, 96.7 %. RF: 0.33. Melting Point: 224 °C

IR ($\nu_{\text{max}}/\text{cm}^{-1}$): 3399 (OH), 3114 (C-H), 1742 (C=O).

^1H NMR (400 MHz, DMSO) δ : 11.12 (s, 1H, -OH), 8.37 – 8.29 (m, 2H, Ar), 7.98 (t, $J = 8.8$ Hz, 1H, Ar), 7.61 – 7.53 (m, 2H, Ar), 6.82 – 6.70 (m, 2H, Ar).

^{13}C NMR (101 MHz, DMSO) δ : 164.83, 164.70, 162.25, 160.96, 160.91, 155.38, 145.07, 134.17, 134.15, 125.27, 123.40, 112.37, 112.34, 107.00, 106.91, 103.93, 103.69.

3-Fluoro-4-nitrophenyl 2-fluoro-4-hydroxybenzoate (**4f**)



Quantities used: compound **3f** (1.26 g, 3.30×10^{-3} mol), PPTS (0.0830 g, 3.30×10^{-4} mol),

ethanol (30 mL), THF (30 mL). The experimental procedure was described in preparation of compound **4a**. Once the reaction was completed, solvent was removed under vacuum and replaced with ethyl acetate. The organic layer was washed with water, brine and dried over MgSO_4 . The solvent was removed to obtain pale yellow solid which was carried forward without further purification.

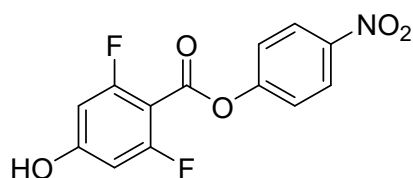
Yield: 0.973 g, 99.5 %. RF: 0.45. Melting Point: 180 °C

IR ($\nu_{\text{max}}/\text{cm}^{-1}$): 3334 (OH), 3101 (C-H), 1706 (C=O).

^1H NMR (400 MHz, DMSO) δ : 11.15 (s, 1H, -OH), 8.29 (t, $J = 8.9$ Hz, 1H, Ar), 7.99 (t, $J = 8.8$ Hz, 1H, Ar), 7.72 (dd, $J = 12.1, 2.4$ Hz, 1H, Ar), 7.46 – 7.38 (m, 1H, Ar), 6.85 – 6.71 (m, 2H, Ar).

^{13}C NMR (101 MHz, DMSO) δ : 164.98, 164.91, 164.85, 162.33, 160.57, 160.52, 156.56, 155.55, 155.44, 153.95, 134.65, 134.57, 134.23, 134.21, 127.49, 127.47, 119.28, 119.24, 112.98, 112.74, 106.73, 106.64, 103.95, 103.72.

4-Nitrophenyl 2,6-difluoro-4-hydroxybenzoate (**4g**)



Quantities used: compound **3g** (0.140 g, 3.69×10^{-4} mol), PPTS (0.00900 g, 3.69×10^{-5} mol), ethanol (20 mL), THF (20 mL). The experimental procedure was described in preparation of compound **4a**. Once the reaction was completed, solvent was removed under vacuum and replaced with ethyl acetate. The organic layer was washed with water, brine and dried over MgSO_4 . The solvent was removed to obtain a white solid which was carried forward without further purification.

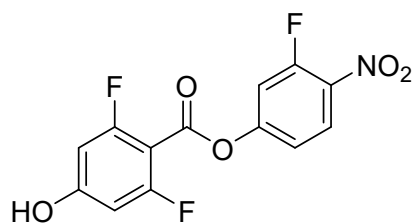
Yield: 0.111 g, 99.5 %. RF: 0.35. Melting Point: 222 °C

IR ($\nu_{\text{max}}/\text{cm}^{-1}$): 3382 (OH), 3116 (C-H), 1748 (C=O).

^1H NMR (400 MHz, DMSO) δ : 11.49 (s, 1H, -OH), 8.36 – 8.32 (m, 2H, Ar), 7.61 – 7.52 (m, 2H, Ar), 6.68 – 6.61 (m, 2H, Ar).

^{13}C NMR (101 MHz, DMSO) δ : 164.02, 163.86, 161.39, 161.31, 154.85, 145.27, 125.43, 123.27, 100.55, 100.28.

3-Fluoro-4-nitrophenyl 2,6-difluoro-4-hydroxybenzoate (**4h**)



Quantities used: compound **3h** (0.260 g, 6.55×10^{-4} mol), PPTS (0.0160 g, 6.55×10^{-5} mol), ethanol (20 mL), THF (20 mL). The experimental procedure was described in preparation of compound **4a**. Once the reaction was completed, solvent was removed under vacuum and replaced with ethyl acetate. The organic layer was washed with water, brine and dried over MgSO_4 . The solvent was removed to obtain pale yellow solid which was carried forward without further purification.

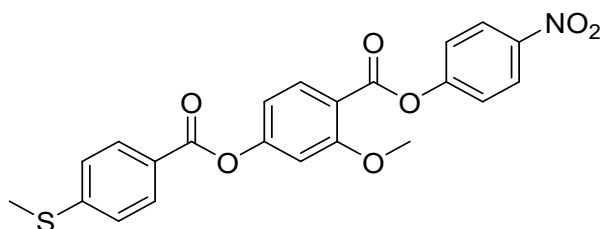
Yield: 0.208 g, 99.2 %. RF: 0.45. Melting Point: 196 °C

IR ($\nu_{\text{max}}/\text{cm}^{-1}$): 3369 (OH), 3110 (C-H), 1739 (C=O).

^1H NMR (400 MHz, DMSO) δ : 11.54 (s, 1H, -OH), 8.29 (t, $J = 8.8$ Hz, 1H, Ar), 7.71 (dd, $J = 12.0, 2.4$ Hz, 1H, Ar), 7.44 – 7.36 (m, 1H, Ar), 6.69 – 6.60 (m, 2H, Ar).

^{13}C NMR (101 MHz, DMSO) δ : 164.99, 164.86, 164.20, 164.12, 164.03, 161.56, 161.48, 158.29, 158.27, 158.24, 156.64, 154.99, 154.88, 154.02, 134.84, 134.77, 127.65, 127.63, 119.10, 119.06, 119.02, 112.87, 112.63, 100.60, 100.57, 100.35, 100.32.

4-Nitrophenyl-2-methoxy-4-((4-methylthio)benzoyl)oxy)benzoate (**5a**)



To a pre-dried flask, 4-(methylthio)benzoic acid (0.323 g, 1.90×10^{-3} mol) was added and dissolved in DCM (50 mL). The addition of DCC (0.430 g, 2.10×10^{-3} mol) was followed by a compound **4a** (0.463 g, 1.60×10^{-3} mol) and the mixture was allowed to stir for 2 min before adding DMAP (0.0200 g, 1.60×10^{-4} mol). The reaction mixture was stirred at room temperature overnight and the extent was monitored by TLC. The white precipitate was removed by filtration and the solvent was evaporated under vacuum to leave crude solid. This was purified using silica chromatography with DCM as the eluent followed by recrystallisation from acetonitrile (20 mL) to obtain a white solid.

Yield: 0.110 g, 15.8 %. RF: 0.55. Melting Point: 164 °C

T_{NI} 172 °C $T_{\text{N}_X\text{N}}$ (97 °C)

IR ($\nu_{\text{max}}/\text{cm}^{-1}$): 2923 (C-H), 1734 (C=O).

^1H NMR (400 MHz, DMSO) δ : 8.36 (d, $J = 8.9$ Hz, 2H, Ar), 8.10 (d, $J = 8.6$ Hz, 1H, Ar), 8.07 (d, $J = 8.3$ Hz, 2H, Ar), 7.60 (d, $J = 8.9$ Hz, 2H, Ar), 7.47 (d, $J = 8.3$ Hz, 2H, Ar), 7.28 (d, $J =$

2.1 Hz, 1H, Ar), 7.08 (dd, $J = 8.6, 2.1$ Hz, 1H, Ar), 3.90 (s, 3H, -OCH₃), 2.58 (s, 3H, -SCH₃).

¹³C NMR (101 MHz, DMSO) δ : 164.27, 162.70, 161.27, 156.41, 156.00, 147.47, 145.56, 133.67, 130.76, 125.79, 125.56, 124.72, 123.88, 115.59, 114.57, 107.78, 56.99, 14.38.

M/Z: [M+H]⁺ Calculated mass for C₂₂H₁₈NO₇S: 440.0801. Found: 440.0804. Difference: -0.7 ppm.

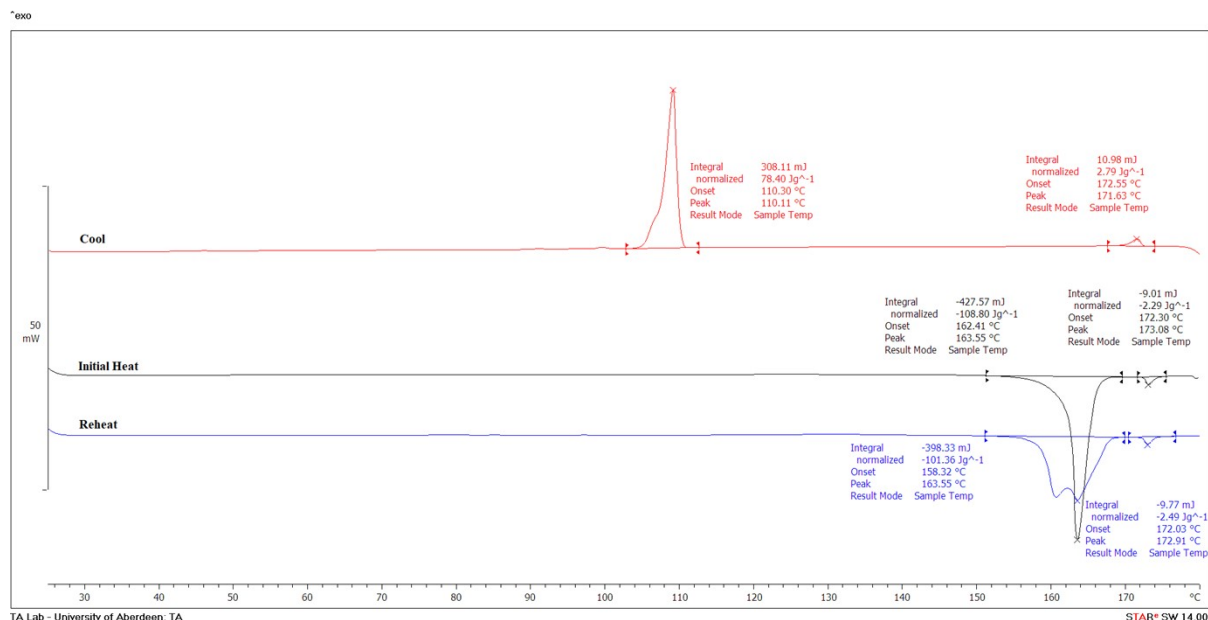
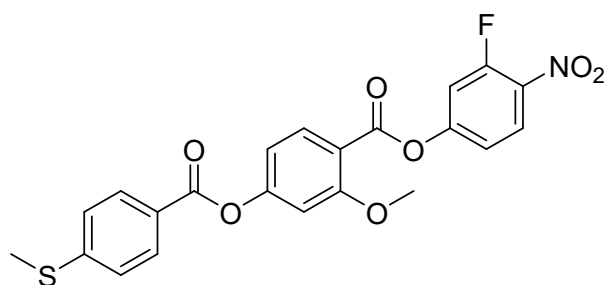


Figure S1. DSC trace for S7.

3-Fluoro-4-nitrophenyl 2-methoxy-4-((4-(methylthio)benzoyl)oxy)benzoate (**5b**)



To a pre-dried flask, 4-(methylthio)benzoic acid (0.300 g, 1.79×10^{-3} mol) was added and dissolved in DCM (50 mL). The reaction mixture was cooled to 0 °C before adding DCC (0.276 g, 1.34×10^{-3} mol) and stirred for 30 min. Compound **4b** (0.411 g, 1.34×10^{-3} mol) was added and stirred overnight at room temperature and the extent was monitored by TLC. The white precipitate was removed by filtration and the solvent was evaporated under vacuum to leave crude solid. This was purified using silica chromatography with DCM as the eluent followed by recrystallisation from acetonitrile (10 mL) to obtain a white solid.

Yield: 0.0300 g, 4.80 %. RF: 0.48. Melting Point: 164 °C

T_{NI} (143 °C) T_{N_FN} (124 °C)

IR ($\nu_{\max}/\text{cm}^{-1}$): 3079 (C-H), 1751 (C=O).

^1H NMR (400 MHz, DMSO) δ : 8.30 (t, $J = 8.9$ Hz, 1H, Ar), 8.10 (d, $J = 8.6$ Hz, 1H, Ar), 8.08 – 8.03 (m, 2H, Ar), 7.73 (dd, $J = 12.0, 2.4$ Hz, 1H, Ar), 7.50 – 7.41 (m, 3H, Ar), 7.28 (d, $J = 2.1$ Hz, 1H, Ar), 7.08 (dd, $J = 8.6, 2.1$ Hz, 1H, Ar), 3.90 (s, 3H, -OCH₃), 2.58 (s, 3H, -SCH₃).

^{13}C NMR (101 MHz, DMSO) δ : 163.80, 161.70, 161.02, 156.62, 156.15, 155.72, 155.61, 154.01, 147.05, 134.65, 134.58, 133.43, 130.31, 127.56, 127.54, 125.09, 124.23, 119.33, 119.29, 114.64, 114.14, 112.99, 112.75, 107.35, 56.55, 13.91.

M/Z: $[\text{M}+\text{H}]^+$ Calculated mass for C₂₂H₁₇NO₇FS: 458.0712. Found: 458.0710. Difference: 0.4 ppm.

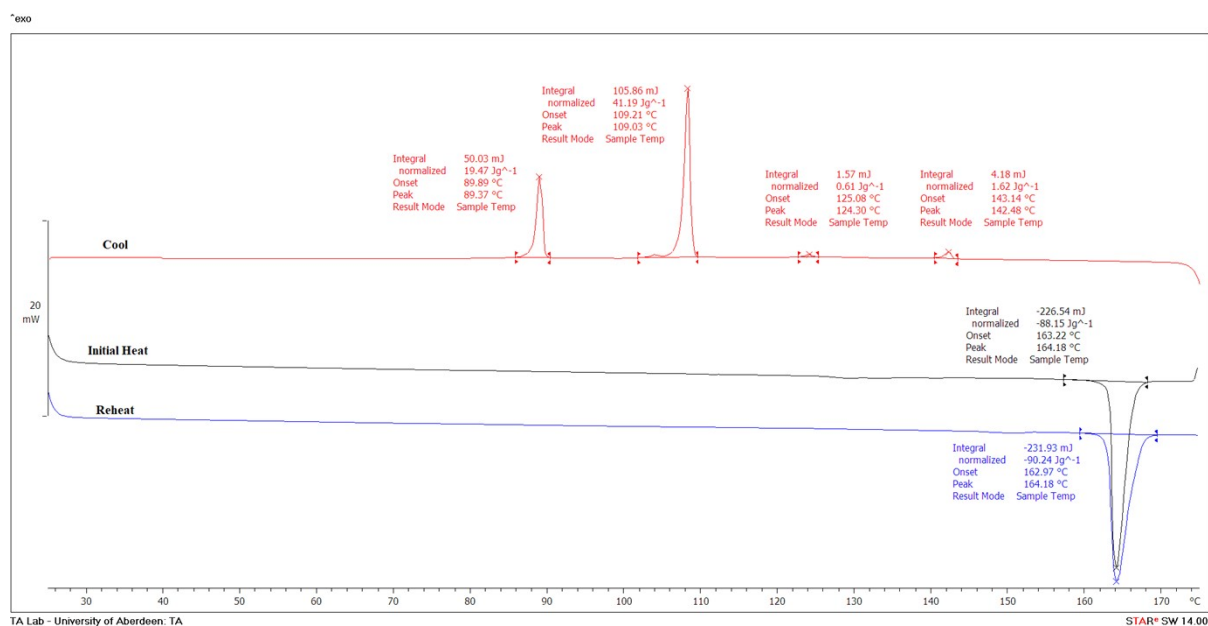
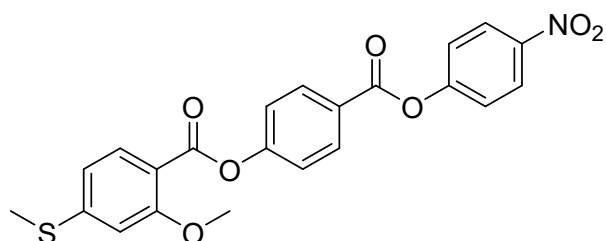


Figure S2. DSC trace for S8.

4-((4-Nitrophenoxy)carbonyl)phenyl 2-methoxy-4-(methylthio)benzoate (**5c**)



Quantities used: 2-methoxy-4-(methylthio)benzoic acid (0.300 g, 1.52×10^{-3} mol), compound **4c** (0.360 g, 1.38×10^{-3} mol), DCC (0.370 g, 1.79×10^{-3} mol), DMAP (0.0200 g, 1.52×10^{-4} mol) and DCM (50 mL). The experimental procedure was described in the preparation of compound **5a**. Purified using column chromatography over silica with DCM as the eluent followed by hot ethanol wash to obtain a white solid.

Yield: 0.290 g, 48.4 %. RF: 0.50. Melting Point: 147 °C

T_{NI} 169 °C T_{N_XN} (111 °C) $T_{N_FN_X}$ (106 °C)

IR (v_{max}/cm^{-1}): 2972 (C-H), 1731 (C=O).

1H NMR (400 MHz, DMSO) δ : 8.41 – 8.33 (m, 2H, Ar), 8.29 – 8.21 (m, 2H, Ar), 7.93 (d, J = 8.3 Hz, 1H, Ar), 7.70 – 7.61 (m, 2H, Ar), 7.54 – 7.46 (m, 2H, Ar), 7.03 (d, J = 1.7 Hz, 1H, Ar), 6.98 (dd, J = 8.3, 1.7 Hz, 1H, Ar), 3.91 (s, 3H, -OCH₃), 2.58 (s, 3H, -SCH₃).

^{13}C NMR (101 MHz, CDCl₃) δ : 163.72, 163.04, 160.62, 155.98, 155.81, 148.53, 145.58, 133.03, 132.05, 125.85, 125.44, 122.79, 122.59, 116.71, 114.08, 109.10, 56.26, 14.97.

M/Z: [M+Na]⁺ Calculated mass for C₂₂H₁₇NO₇SNa: 462.0644 Found: 462.0623. Difference: 4.5 ppm.

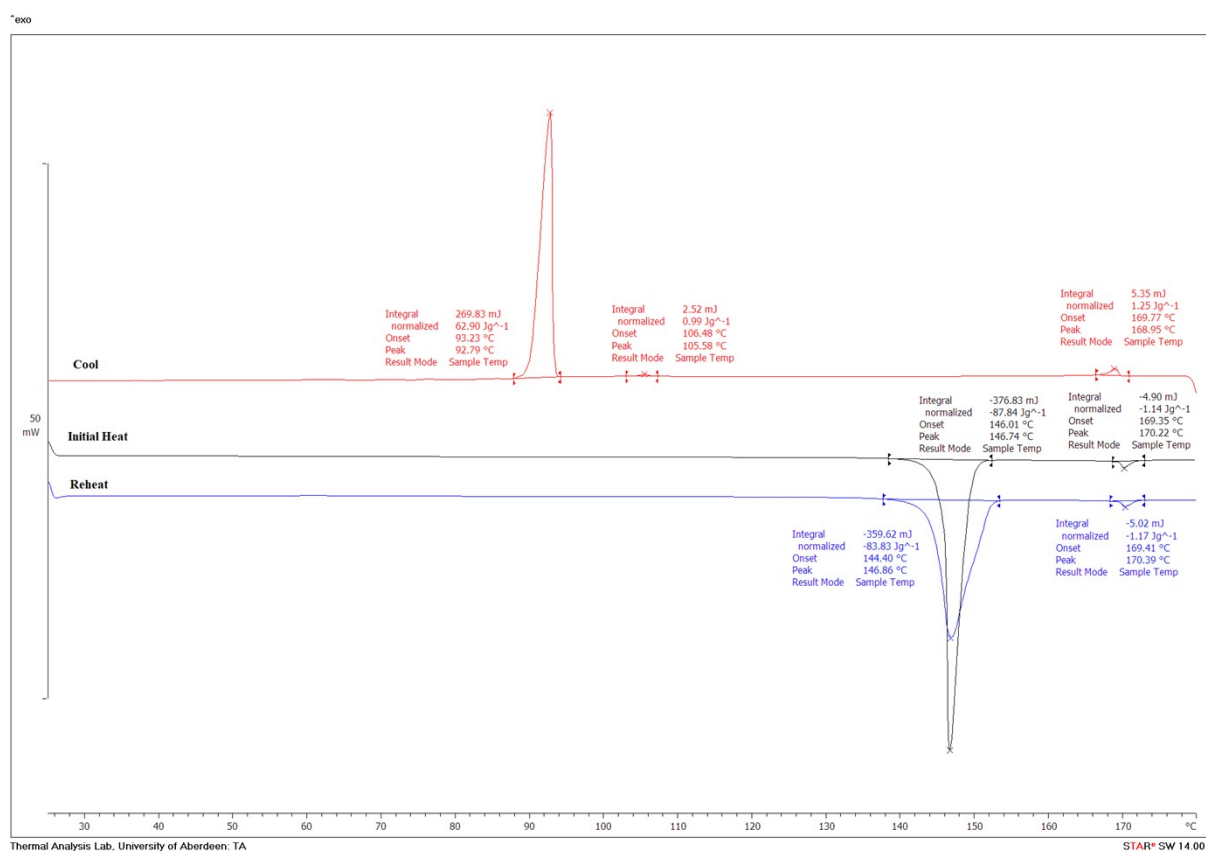
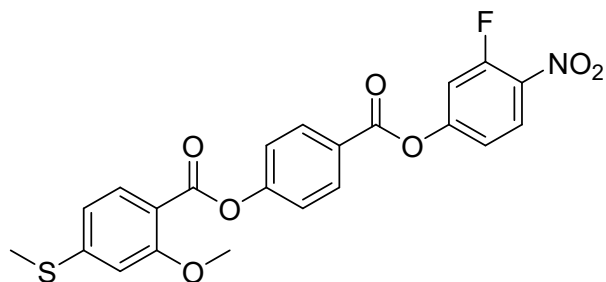


Figure S3. DSC trace for S1.

4-((3-Fluoro-4-nitrophenoxy)carbonyl)phenyl 2-methoxy-4-(methylthio)benzoate (**5d**)



Quantities used: 2-methoxy-4-(methylthio)benzoic acid (0.300 g, 1.52×10^{-3} mol), compound **4d** (0.380 g, 1.38×10^{-3} mol), DCC (0.370 g, 1.79×10^{-3} mol), DMAP (0.0200 g, 1.52×10^{-4} mol) and DCM (50 mL). The experimental procedure was described in the preparation of compound **5a**. Purified using column chromatography over silica with DCM as the eluent followed by hot ethanol wash to obtain a yellow solid.

Yield: 0.228 g, 36.2 %. RF: 0.50. Melting Point: 147 °C

T_{NI} (135 °C) T_{NPN} (122 °C)

IR (ν_{max}/cm^{-1}): 2988 (C-H), 1739 (C=O).

^1H NMR (400 MHz, DMSO) δ : 8.32 (t, $J = 8.9$ Hz, 1H, Ar), 8.28 – 8.20 (m, 2H, Ar), 7.93 (d, $J = 8.3$ Hz, 1H, Ar), 7.79 (dd, $J = 12.0, 2.4$ Hz, 1H, Ar), 7.55 – 7.46 (m, 3H, Ar), 7.03 (d, $J = 1.7$ Hz, 1H, Ar), 6.98 (dd, $J = 8.4, 1.7$ Hz, 1H, Ar), 3.91 (s, 3H, -OCH₃), 2.58 (s, 3H, -SCH₃).

^{13}C NMR (101 MHz, CDCl₃) δ : 163.13, 162.86, 160.51, 157.56, 156.04, 155.82, 155.71, 154.91, 148.48, 134.91, 134.84, 132.91, 131.99, 127.27, 127.25, 125.28, 122.55, 118.14, 118.10, 116.58, 113.88, 112.54, 112.30, 108.96, 56.14, 14.84.

M/Z: $[\text{M}+\text{Na}]^+$ Calculated mass for C₂₂H₁₆NO₇FSNa: 480.0537. Found: 480.0529. Difference: 1.7 ppm.

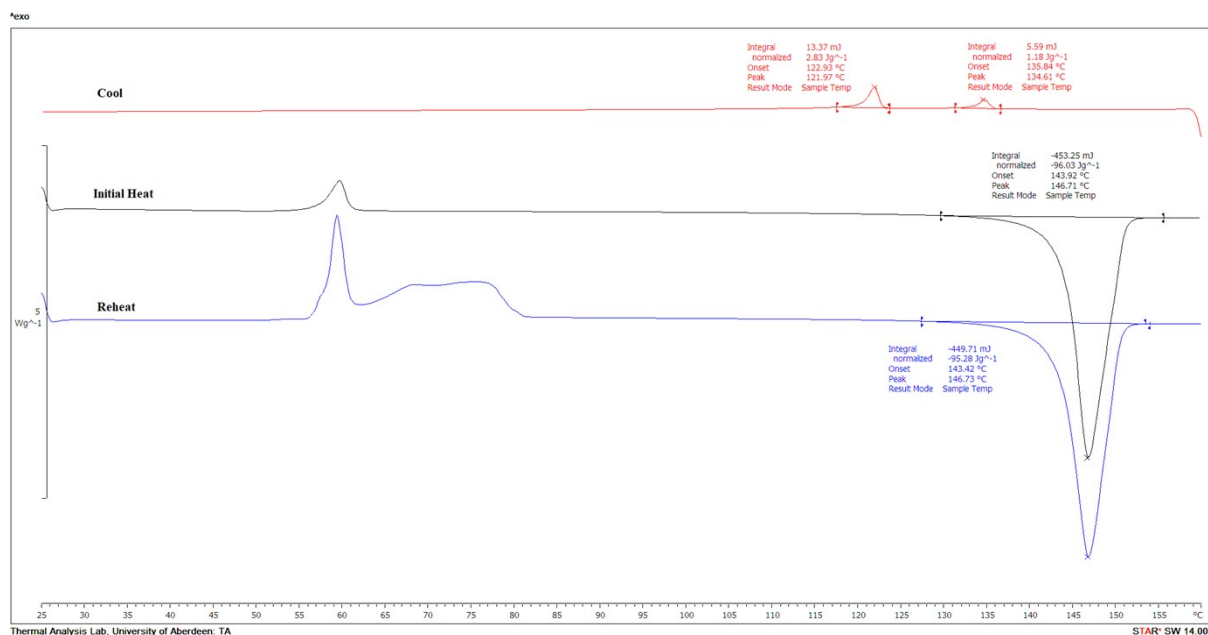
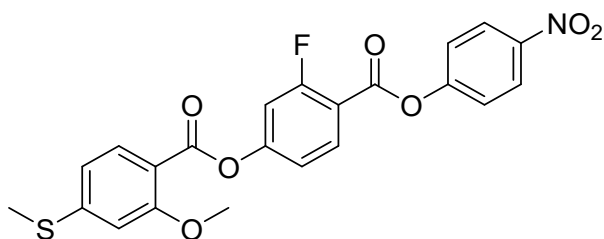


Figure S4. DSC trace for S2.

3-Fluoro-4-((4-nitrophenoxy)carbonyl)phenyl 2-methoxy-4-(methylthio)benzoate (**5e**)



Quantities used: 2-methoxy-4-(methylthio)benzoic acid (0.300 g, 1.52×10^{-3} mol), compound **4e** (0.315 g, 1.14×10^{-3} mol), DCC (0.234 g, 1.14×10^{-3} mol) and DCM (50 mL). The experimental procedure was described in the preparation of compound **5b**. Purified using column chromatography over silica with DCM as the eluent followed by hot ethanol wash to obtain a white solid.

Yield: 0.197 g, 38.3 %. RF: 0.54. Melting Point: 162 °C

T_{NI} (152 °C) $T_{N_F,N}$ (126 °C)

IR (ν_{max}/cm^{-1}): 3073 (C-H), 1728 (C=O).

1H NMR (400 MHz, DMSO) δ : 8.40 – 8.34 (m, 2H, Ar), 8.23 (t, $J = 8.5$ Hz, 1H, Ar), 7.94 (d, $J = 8.3$, 1H, Ar), 7.69 – 7.63 (m, 2H, Ar), 7.53 (dd, $J = 11.7, 2.2$ Hz, 1H, Ar), 7.39 – 7.34 (m, 1H, Ar), 7.05 – 6.96 (m, 2H, Ar), 3.91 (s, 3H, -OCH₃), 2.59 (s, 3H, -SCH₃).

^{13}C NMR (101 MHz, DMSO) δ : 163.34, 162.01, 160.75, 160.67, 159.93, 156.22, 156.10, 155.12, 148.34, 145.32, 133.49, 132.51, 125.37, 123.43, 118.99, 118.95, 116.55, 114.36, 114.27, 112.90, 111.94, 111.69, 108.97, 56.13, 13.96.

M/Z: $[M+H]^+$ Calculated mass for C₂₂H₁₇NO₇FS: 458.0708. Found: 458.0710. Difference: -0.4 ppm.

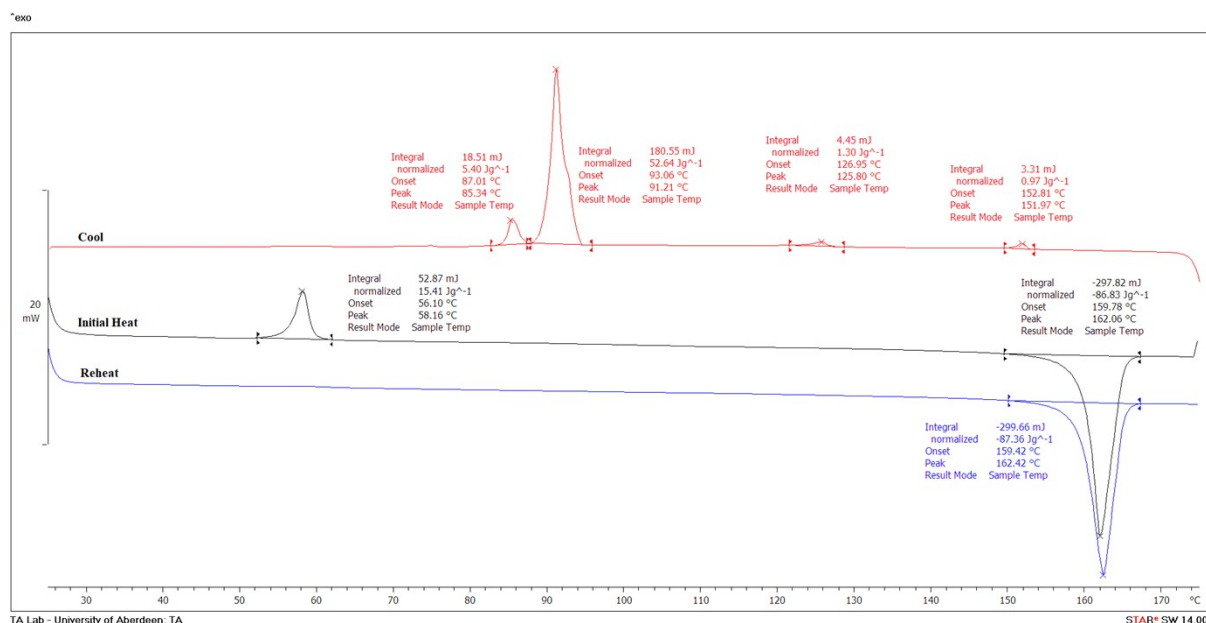
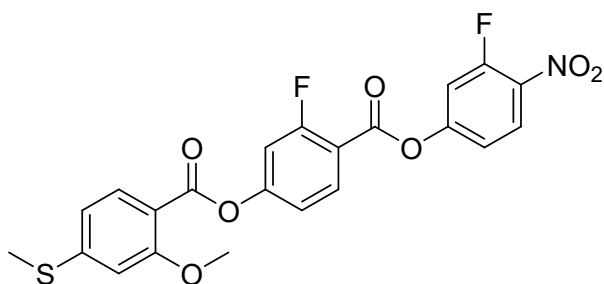


Figure S5. DSC trace for S3.

3-Fluoro-4-((3-fluoro-4-nitrophenoxy)carbonyl)phenyl 2-methoxy-4-(methylthio)benzoate
(5f)



Quantities used: 2-methoxy-4-(methylthio)benzoic acid (0.300 g, 1.52×10^{-3} mol), compound **4f** (0.335 g, 1.14×10^{-3} mol), DCC (0.234 g, 1.14×10^{-3} mol) DCM (30 mL). The experimental procedure was described in the preparation of compound **5b**. Purified using column chromatography over silica with DCM as the eluent followed by hot ethanol wash to obtain a white solid.

Yield: 0.104 g, 19.3 %. RF: 0.38. Melting Point: 150 °C

T_{NfI} (129 °C)

IR (ν_{max}/cm^{-1}): 3056 (C-H), 1727 (C=O).

1H NMR (400 MHz, DMSO) δ : 8.33 (t, $J = 8.8$ Hz, 1H, Ar), 8.22 (t, $J = 8.5$ Hz, 1H, Ar), 7.94 (d, $J = 8.3$ Hz, 1H, Ar), 7.79 (dd, $J = 11.9, 2.3$ Hz, 1H, Ar), 7.56 – 7.47 (m, 2H, Ar), 7.37 (dd, $J = 8.6, 2.1$ Hz, 1H, Ar), 7.05 – 6.96 (m, 2H, Ar), 3.91 (s, 3H, -OCH₃), 2.59 (s, 3H, -SCH₃).

^{13}C NMR (101 MHz, DMSO) δ : 163.40, 161.97, 160.80, 160.24, 159.94, 156.53, 156.35, 156.24, 155.22, 155.11, 153.91, 148.37, 134.91, 134.84, 133.54, 132.51, 127.61, 127.59, 119.30, 119.26, 119.03, 118.99, 116.54, 114.07, 113.99, 113.01, 112.86, 112.77, 111.98, 111.73, 108.96, 56.13, 13.95.

M/Z: $[M+Na]^+$ Calculated mass for C₂₂H₁₅NO₇F₂NaS: 498.0415. Found: 498.0435. Difference: -4.0 ppm.

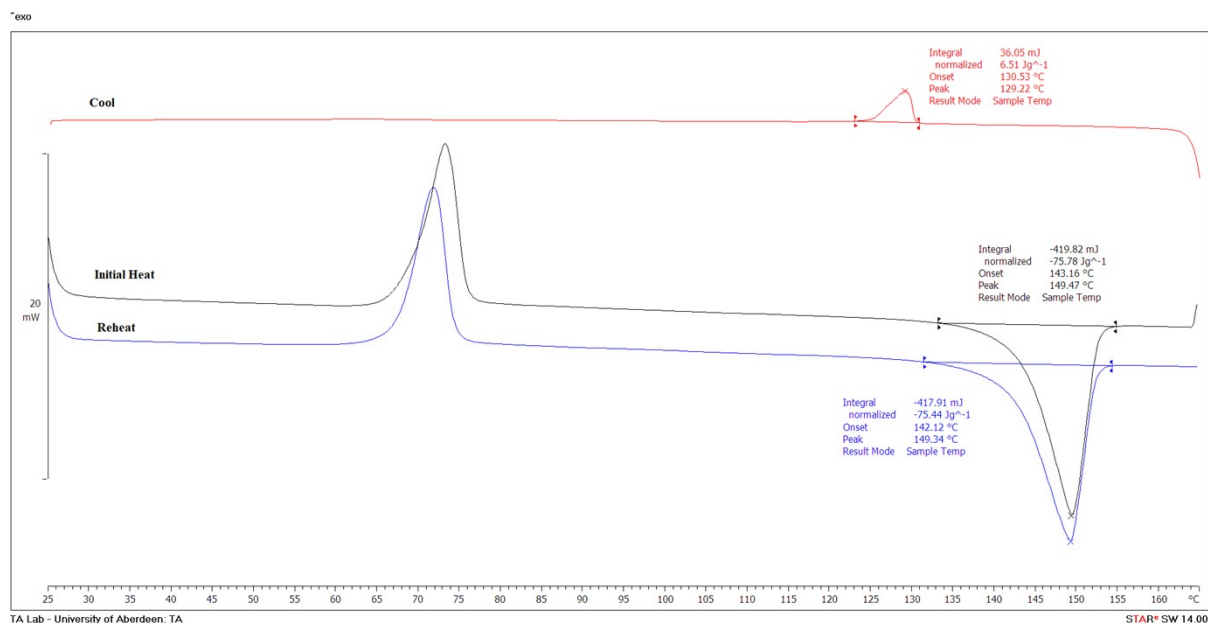
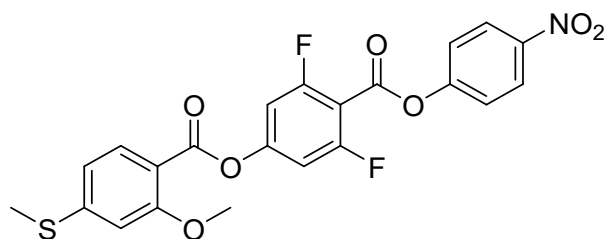


Figure S6. DSC trace for S4.

4-Nitrophenyl 2,6-difluoro-4-((2-methoxy-4-(methylthio)benzoyl)oxy)benzoate (**5g**)



Quantities used: 2-methoxy-4-(methylthio)benzoic acid (0.134 g, 6.78×10^{-4} mol), compound **4g** (0.100 g, 3.99×10^{-4} mol), DCC (0.0700 g, 3.39×10^{-4} mol) and DCM/THF (45/5 mL). The experimental procedure was described in the preparation of compound **5b**. Purified using column chromatography over silica with DCM as the eluent followed by hot ethanol wash to obtain a white solid.

Yield: 0.0370 g, 23.0 %. RF: 0.38. Melting Point: 174 °C

T_{NI} (127 °C) $T_{NF,N}$ (121 °C)

IR (ν_{max}/cm^{-1}): 3070 (C-H), 1731 (C=O).

1H NMR (400 MHz, $CDCl_3$) δ : 8.36 – 8.31 (m, 2H, Ar), 7.96 (d, $J = 8.1$ Hz, 1H, Ar), 7.49 – 7.44 (m, 2H, Ar), 7.06 – 7.00 (m, 2H, Ar), 6.90 – 6.85 (m, 2H, Ar), 3.96 (s, 3H, -OCH₃), 2.56 (s, 3H, -SCH₃).

^{13}C NMR (101 MHz, $CDCl_3$) δ : 163.20, 163.13, 162.07, 160.78, 160.62, 160.55, 158.64, 155.70, 155.56, 155.41, 155.04, 149.35, 145.82, 133.04, 125.47, 122.69, 116.68, 113.08, 108.97, 107.43, 107.40, 107.18, 107.14, 106.69, 106.53, 106.37, 56.24, 14.90.

M/Z: $[M+H]^+$ Calculated mass for $C_{22}H_{16}NO_7F_2S$: 476.0611. Found: 476.0616. Difference: -1.1 ppm.

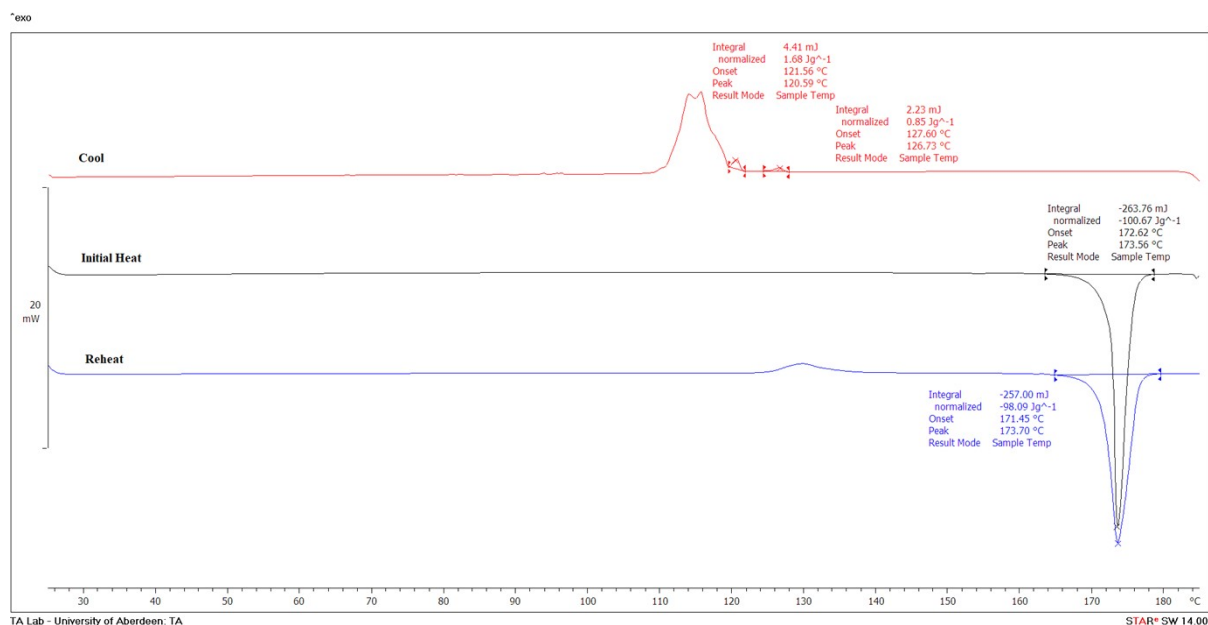
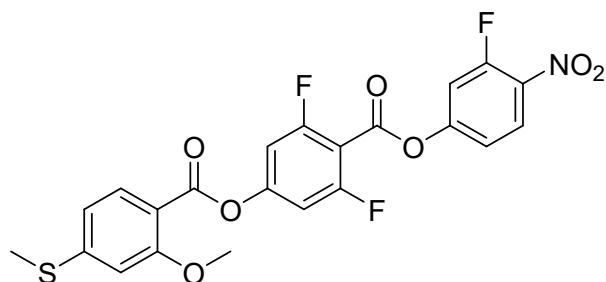


Figure S7. DSC trace for S5.

3-Fluoro-4-nitrophenyl 2,6-difluoro-4-((2-methoxy-4-(methylthio)benzoyl)oxy)benzoate (**5h**)



Quantities used: 2-methoxy-4-(methylthio)benzoic acid (0.182 g , $9.20 \times 10^{-3}\text{ mol}$), compound **4h** (0.144 g , $4.60 \times 10^{-3}\text{ mol}$), DCC (0.0950 g , $4.60 \times 10^{-3}\text{ mol}$) and DCM/THF ($45/5\text{ mL}$). The experimental procedure was described in the preparation of compound **5b**. Purified using column chromatography over silica with DCM as the eluent followed by hot ethanol wash to obtain a white solid.

Yield: 0.0690 g , 30.4 %. RF: 0.53. Melting Point: $171\text{ }^\circ\text{C}$

T_{NFI} ($122\text{ }^\circ\text{C}$)

IR ($\nu_{\max}/\text{cm}^{-1}$): 3056 (C-H), 1730 (C=O).

$^1\text{H NMR}$ (400 MHz, CDCl_3) δ : 8.20 (t, $J = 8.6\text{ Hz}$, 1H, Ar), 7.96 (d, $J = 8.1\text{ Hz}$, 1H, Ar), 7.33 (dd, $J = 11.1, 2.4\text{ Hz}$, 1H, Ar), 7.29 – 7.27 (m, 1H, Ar), 7.07 – 7.00 (m, 2H, Ar), 6.90 – 6.85 (m, 2H, Ar), 3.96 (s, 3H, -OCH₃), 2.56 (s, 3H, -SCH₃).

^{13}C NMR (101 MHz, CDCl_3) δ : 163.17, 163.09, 161.90, 160.68, 160.58, 160.51, 158.03, 157.51, 155.86, 155.71, 155.56, 154.94, 154.85, 154.84, 149.31, 135.18, 135.11, 132.92, 127.32, 127.30, 118.02, 117.98, 116.56, 112.89, 112.47, 112.23, 108.84, 107.38, 107.34, 107.12, 107.09, 105.95, 56.12, 14.78.

M/Z: $[\text{M}+\text{H}]^+$ Calculated mass for $\text{C}_{22}\text{H}_{15}\text{NO}_7\text{F}_3\text{S}$: 494.0512. Found: 494.0521. Difference: -1.8 ppm.

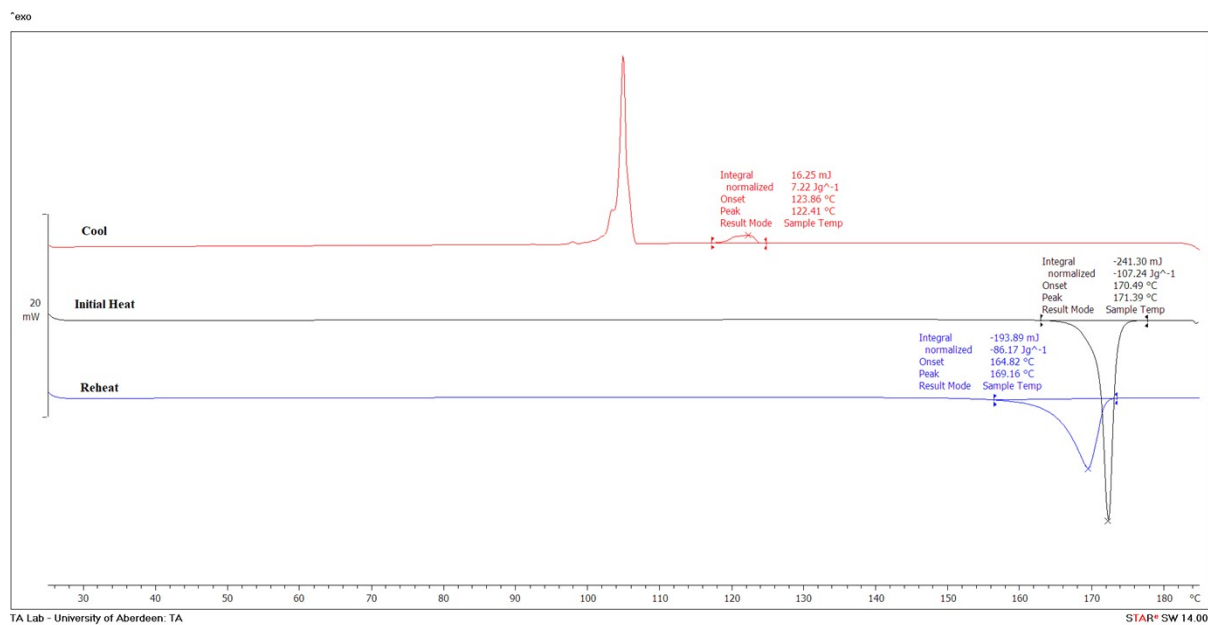
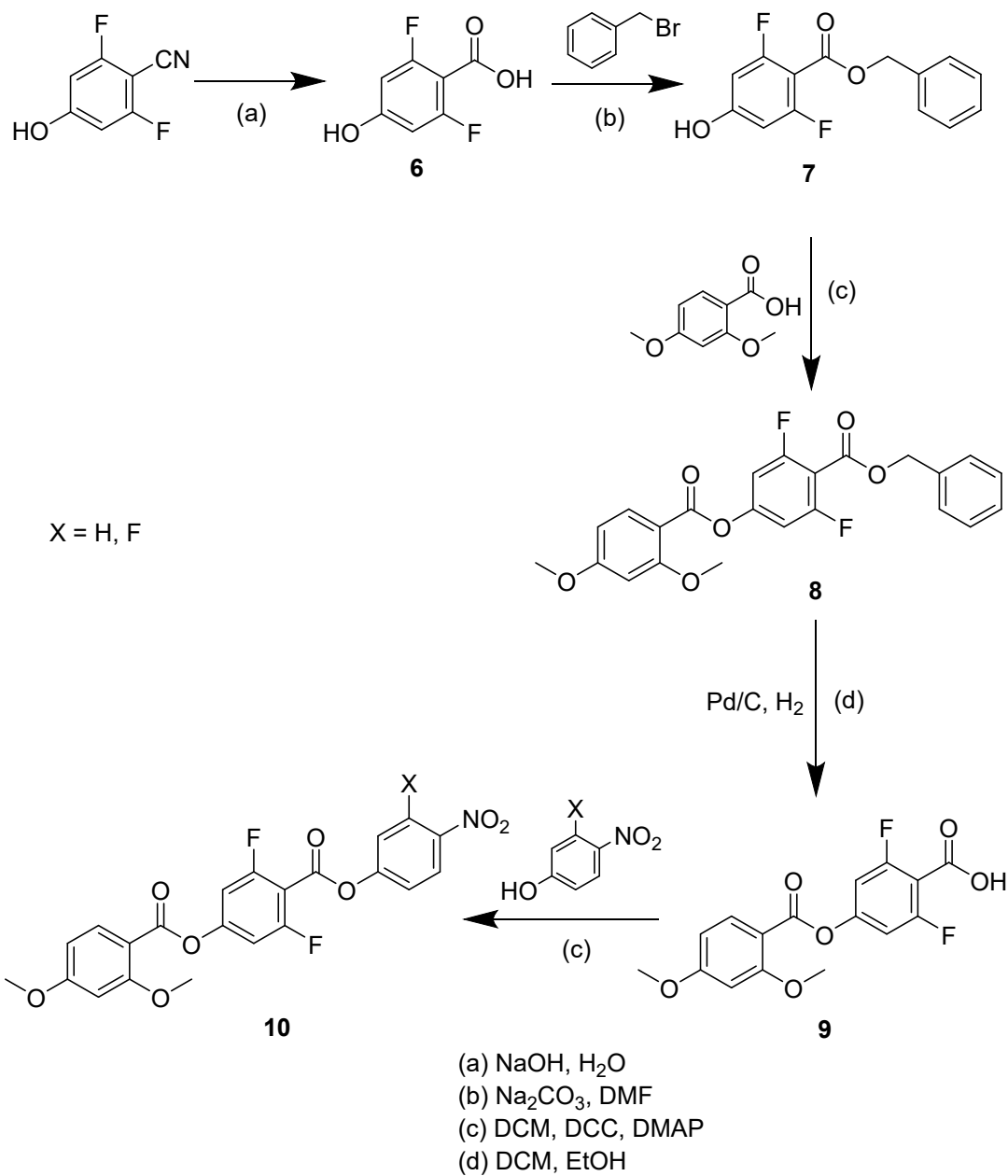
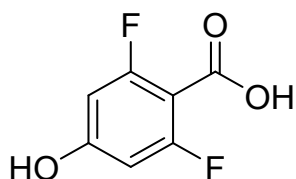


Figure S8. DSC trace for S6.



Scheme 2. Synthetic route used to obtain O5 and O6.

2,6-Difluoro-4-hydroxybenzoic acid (**6**)



2,6-Difluoro-4-hydroxybenzotrile (19.0 g, 1.23×10^{-1} mol) was dissolved in water (150 mL) while stirring. Sodium hydroxide (15.0 g, 3.80×10^{-1} mol) was carefully dissolved in water (150 ml) and added to the solution. The solution was then left stirring at reflux overnight. Reaction progress was monitored using thin layer chromatography using petroleum ether (40-60) (70%) and ethyl acetate (30%) as eluent. After cooling to room temperature, the solution was acidified using 1M HCl solution, it was then extracted using ethyl acetate. The ethyl acetate was removed under vacuum to afford the crude product, which was then recrystallised using water. Solid was redissolved in ethyl acetate, dried with MgSO_4 , and concentrated under vacuum to afford a white solid.

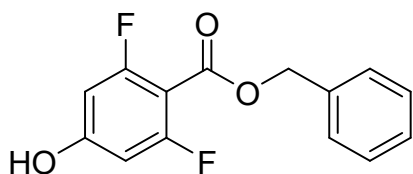
Yield: 9.26 g, 47.0 %. RF: 0.030. Melting Point: 198 °C

IR ($\nu_{\text{max}}/\text{cm}^{-1}$): 3535 (OH), 3081 (OH), 1687 (C=O).

^1H NMR (400 MHz, DMSO) δ : 13.17 (s, 1H, -COOH), 11.00 (s, 1H, -OH), 6.55 – 6.45 (m, 2H, Ar).

^{13}C NMR (101 MHz, DMSO) δ : 162.78, 162.68, 162.35, 162.33, 162.32, 161.83, 161.68, 161.53, 160.28, 160.18, 102.44, 102.26, 102.08, 99.89, 99.87, 99.82, 99.68, 99.64, 99.61.

Phenyl 2,6-difluoro-4-hydroxybenzoate (**7**)



Compound **6** (5.00 g, 2.87×10^{-2} mol) and Na_2CO_3 (3.04 g, 2.87×10^{-2} mol) were first azeotroped in dry toluene three times. Following this, dry DMF (50 ml) was added. Benzyl bromide (3.40 mL, 4.91 g, 2.87×10^{-2} mol) was added and the mixture was left stirring at room temperature overnight. The mixture was added to distilled water (200 mL) and acidified to approximately pH 4 using dilute HCl. It was extracted using diethyl ether (5 x 25 mL). The combined organic extracts were washed using water and brine before finally being dried over magnesium sulfate. The crude product was purified by flash chromatography using petroleum ether (40-60) (70%) and ethyl acetate (30%) as eluent. The residue was recrystallised from toluene (30 mL) to obtain a white solid.

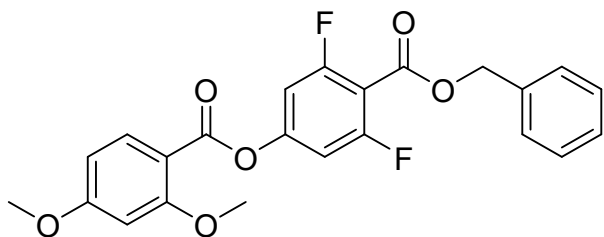
Yield: 2.86 g, 38.0 %. RF: 0.40. Melting Point: 163 °C

IR ($\nu_{\text{max}}/\text{cm}^{-1}$): 3182 (OH), 1672 (C=O).

^1H NMR (400 MHz, DMSO) δ : 11.17 (s, 1H, -OH), 7.46 – 7.29 (m, 5H, Ar), 6.60 – 6.50 (m, 2H, Ar), 5.31 (s, 2H, (C=O)-O-CH₂-).

^{13}C NMR (101 MHz, DMSO) δ : 163.05, 162.96, 162.70, 162.55, 162.40, 160.75, 160.73, 160.71, 160.53, 160.44, 135.78, 128.49, 128.13, 127.91, 100.73, 100.56, 100.39, 100.14, 100.11, 100.07, 99.89, 99.86, 66.49.

Phenyl 4-((2,4-dimethoxybenzoyl)oxy)-2,6-difluorobenzoate (**8**)



2,4-Dimethoxybenzoic acid (0.860 g, 4.70×10^{-3} mmol) and DCC (1.14 g, 5.5×10^{-3} mol) were dissolved in DCM (50 mL) and left stirring for 10 min. Compound **7** (1.13 g, 4.27×10^{-3} mol) and DMAP (0.520 g, 0.430×10^{-3} mol) were added together, and the mixture was left stirring at room temperature overnight. The mixture was filtered to remove the dicyclohexylurea. The crude product was purified by flash chromatography using DCM (98%) and ethyl acetate (2%) as eluent to obtain a white solid.

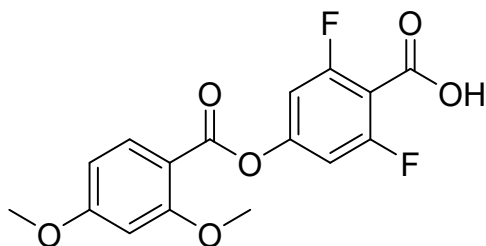
Yield: 1.19 g. 65.0 %. RF: 0.71. Melting Point: 101 °C

IR ($\nu_{\text{max}}/\text{cm}^{-1}$): 3016 (C-H), 1727 (C=O).

^1H NMR (400 MHz, DMSO) δ : 7.97 (d, $J = 8.8$ Hz, 1H, Ar), 7.50 – 7.28 (m, 7H, Ar), 6.71 (d, $J = 2.3$ Hz, 1H, Ar), 6.68 (dd, $J = 8.8, 2.4$ Hz, 1H, Ar), 5.41 (s, 2H, (C=O)-O-CH₂-), 3.88 (s, 3H, -OCH₃), 3.87 (s, 3H, -OCH₃).

^{13}C NMR (101 MHz, DMSO) δ : 165.32, 162.13, 161.49, 161.46, 161.37, 160.23, 158.93, 158.85, 154.51, 154.36, 154.21, 135.35, 134.34, 128.55, 128.33, 128.08, 108.93, 107.88, 107.84, 107.70, 107.63, 107.59, 107.52, 107.34, 105.84, 98.98, 67.29, 56.03, 55.78.

4-((2,4-Dimethoxybenzoyl)oxy)-2,6-difluorobenzoic acid (**9**)



Compound **8** (1.14 g, 2.66×10^{-3} mol) was dissolved in a 50:50 mixture of DCM and ethanol (100 mL). This solution was first evacuated under vacuum and purged with argon. Pd/C 5% (0.0140g, 0.130×10^{-3} mol) was added, the argon atmosphere was replaced with hydrogen gas and the mixture was left stirring at room temperature overnight. Hydrogen was pumped out of

the system and the flask was purged thoroughly with argon. Reaction progress was monitored using thin layer chromatography using DCM (98%) and ethyl acetate (2%) as eluent. The mixture was filtered through Celite and the solvents were removed under vacuum to obtain a white solid which was used without further purification.

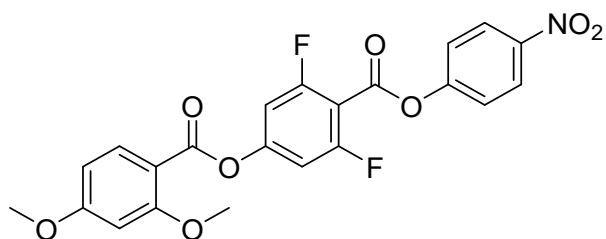
Yield: 0.730 g, 81.0 %. RF: 0.010. Melting Point: 204 °C

IR ($\nu_{\max}/\text{cm}^{-1}$): 2847 (OH), 1757 (C=O).

^1H NMR (400 MHz, DMSO) δ : 13.84 (s, 1H, -COOH), 7.97 (d, J = 8.7 Hz, 1H, Ar), 7.29 – 7.20 (m, 2H, Ar), 6.71 (d, J = 2.2 Hz, 1H, Ar), 6.67 (dd, J = 8.6, 2.4 Hz, 1H, Ar), 3.88 (s, 3H, -OCH₃), 3.87 (s, 3H, -OCH₃).

^{13}C NMR (101 MHz, DMSO) δ : 165.26, 162.07, 161.83, 161.71, 160.92, 160.82, 158.42, 158.32, 153.38, 153.23, 153.09, 134.30, 110.11, 109.91, 109.10, 107.54, 107.51, 107.47, 107.28, 107.25, 105.82, 98.99, 56.04, 55.78.

4-Nitrophenyl 4-((2,4-dimethoxybenzoyl)oxy)-2,6-difluorobenzoate (**10a**)



Compound **9** (0.540 g, 1.60×10^{-3} mol) and DCC (0.170 g, 0.800×10^{-3} mol) were dissolved in DCM (50 mL) at 0° and were left stirring for 20 min. 4-nitrophenol (0.110 g, 0.800×10^{-3} mmol) was added and the mixture was left stirring at room temperature overnight. The solvent was removed under vacuum and the crude product was purified by flash chromatography using DCM as the eluent. The residue was washed with hot ethanol to obtain a white solid.

Yield: 0.0550 g, 15.0 %. RF: 0.34. Melting Point: 192 °C

T_{NI} (139 °C) $T_{\text{NF,N}}$ (132 °C)

IR ($\nu_{\max}/\text{cm}^{-1}$): 3123 (C-H), 1754 (C=O).

^1H NMR (400 MHz, CDCl₃) δ : 8.38 – 8.29 (m, 2H, Ar), 8.04 (d, J = 8.8 Hz, 1H, Ar), 7.51 – 7.43 (m, 2H, Ar), 7.06 – 7.00 (m, 2H, Ar), 6.58 (dd, J = 8.8, 2.3 Hz, 1H, Ar), 6.54 (d, J = 2.3 Hz, 1H, Ar), 3.95 (s, 3H, -OCH₃), 3.91 (s, 3H, -OCH₃).

^{13}C NMR (101 MHz, CDCl₃) δ : 165.94, 163.23, 163.15, 162.93, 161.96, 160.65, 160.58, 158.71, 155.75, 155.08, 145.83, 134.88, 125.49, 122.71, 109.61, 107.48, 107.44, 107.23, 107.19, 106.40, 105.31, 99.16, 56.21, 55.84.

M/Z: $[\text{M}+\text{H}]^+$ Calculated mass for C₂₂H₁₆NO₈F₂: 460.0825. Found: 460.0844. Difference: -4.1 ppm.

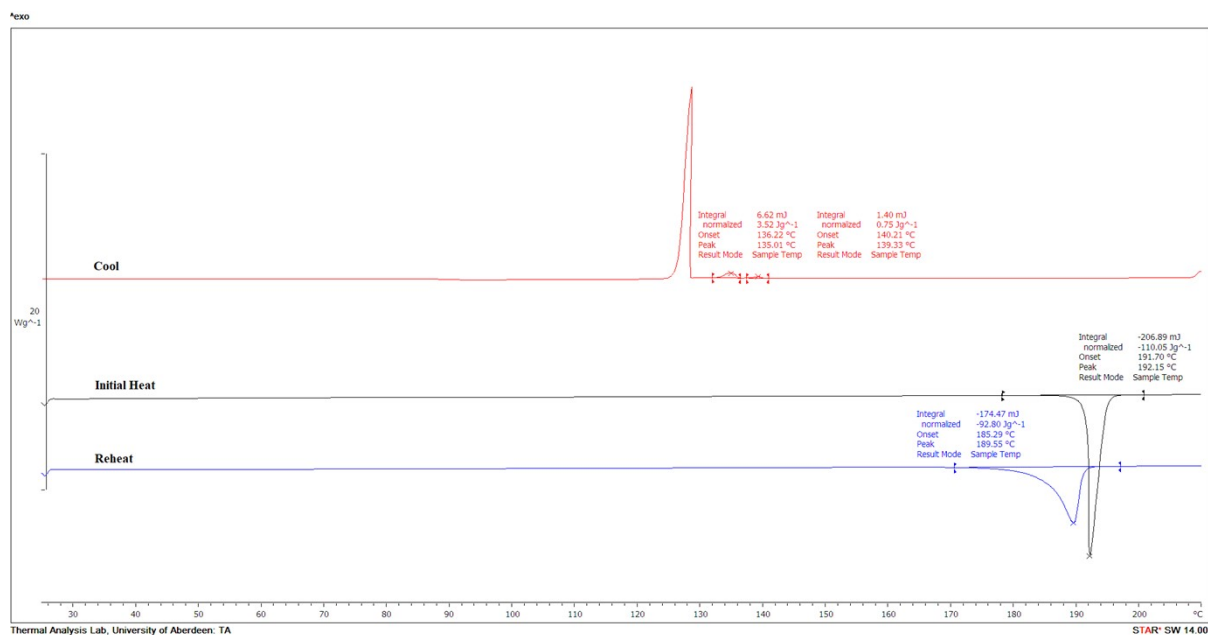
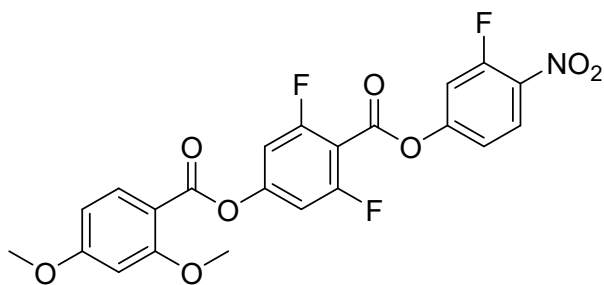


Figure S9. DSC trace for O5.

3-Fluoro-4-nitrophenyl 4-((2,4-dimethoxybenzoyl)oxy)-2,6-difluorobenzoate (**10b**)



Compound **9** (0.600 g, 1.78×10^{-3} mol) and DCC (0.180 g, 0.890×10^{-3} mol) were dissolved in DCM (50 mL) at 0 °C and were left stirring for 20 min. 3-Fluoro-4-nitrophenol (0.140 g, 0.890×10^{-3} mol) was added and the mixture was left stirring at room temperature overnight. The solvent was removed under vacuum and the crude product was purified by flash chromatography using DCM as the eluent. The residue was washed with hot ethanol to produce a white solid.

Yield: 0.0440 g, 10.0 %. RF: 0.43. Melting Point: 160 °C

T_{NFI} (131 °C)

IR (ν_{max}/cm^{-1}): 3112 (C-H), 1745 (C=O).

^1H NMR (400 MHz, CDCl_3) δ : 8.19 (t, $J = 8.7$ Hz, 1H, Ar), 8.03 (d, $J = 8.6$ Hz, 1H, Ar), 7.32 (dd, $J = 11.2, 2.4$ Hz, 1H, Ar), 7.29 – 7.22 (m, 1H, Ar), 7.06 – 6.98 (m, 2H, Ar), 6.56 (dd, $J = 8.9, 2.3$ Hz, 1H, Ar), 6.54 (d, $J = 2.2$ Hz, 1H, Ar), 3.94 (s, 3H, -OCH₃), 3.90 (s, 3H, -OCH₃).

^{13}C NMR (101 MHz, CDCl_3) δ : 165.96, 163.29, 163.22, 162.93, 161.88, 160.71, 160.64, 158.20, 157.63, 156.16, 156.02, 155.87, 155.09, 154.99, 154.97, 135.28, 135.21, 134.87,

127.43, 127.41, 118.16, 118.11, 112.59, 112.35, 109.50, 107.52, 107.49, 107.27, 107.23, 105.89, 105.33, 99.13, 56.19, 55.82.

M/Z: [M+H]⁺ Calculated mass for C₂₂H₁₅NO₈F₃: 478.0727. Found: 478.0750. Difference: -4.8 ppm.

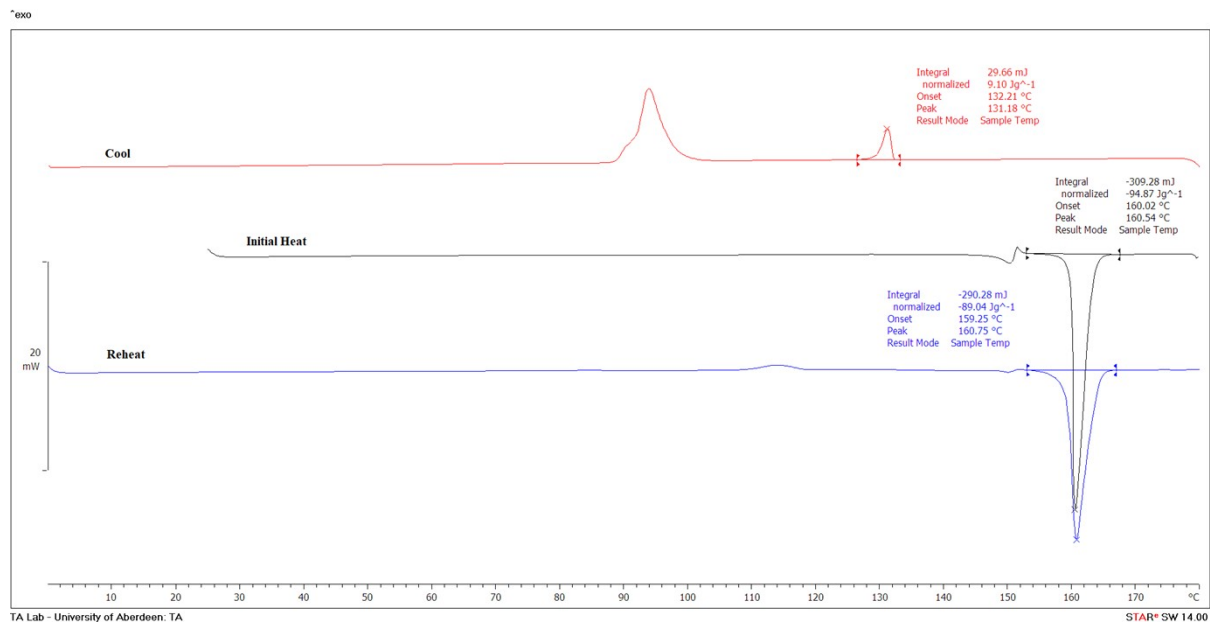


Figure S10. DSC trace for O6.